Journal of Sound and Vibration 511 (2021) 116331

Contents lists available at ScienceDirect

Journal of Sound and Vibration

journal homepage: www.elsevier.com/locate/jsvi

Computational inference of vibratory system with incomplete modal information using parallel, interactive and adaptive Markov chains

K. Zhou [a], J. Tang [b,*]

[a] Department of Mechanical Engineering-Engineering Mechanics, Michigan Technological University, USA
[b] Department of Mechanical Engineering, University of Connecticut, 191 Auditorium Road, Unit 3139, Storrs, CT 06269, USA

ARTICLE INFO

Handling Editor: Eleni Chatzi

Keywords:
Inverse analysis
Incomplete modal information
Uncertainties
Bayesian inference
Parallel, interactive and adaptive Markov chains
Multiple local optima

ABSTRACT

Inverse analysis of vibratory system is an important subject in fault identification, model updating, and robust design and control. It is challenging subject because 1) the problem is oftentimes underdetermined while the measurements are limited and/or incomplete; 2) many combinations of parameters may yield results that are similar with respect to actual response measurements; and 3) uncertainties inevitably exist. The aim of this research is to leverage upon computational intelligence through statistical inference to facilitate an enhanced, probabilistic framework using incomplete modal response measurement. This new framework is built upon efficient inverse identification through optimization, whereas Bayesian inference is employed to account for the effect of uncertainties. To overcome the computational cost barrier, we adopt Markov chain Monte Carlo (MCMC) to characterize the target function/distribution. Instead of using single Markov chain in conventional Bayesian approach, we develop a new sampling theory with multiple parallel, interactive and adaptive Markov chains and incorporate it into Bayesian inference. This can harness the collective power of these Markov chains to realize the concurrent search of multiple local optima. The number of required Markov chains and their respective initial model parameters are automatically determined via Monte Carlo simulation-based sample pre-screening followed by *K*-means clustering analysis. These enhancements can effectively address the aforementioned challenges in finite element inverse analysis. The validity of this framework is systematically demonstrated through case studies.

1. Introduction

Finite element (FE) method nowadays is pervasive in the design, monitoring and control of mechanical structures [1–4]. Finite element inverse analysis is an important subject in which the root cause of the discrepancy between the FE-based response prediction and the actual measurement or desired/target response is elucidated. Typically, in an inverse analysis, certain modeling parameters are identified/updated to facilitate model updating, design optimization, or fault identification [2–4]. In dynamic systems, FE inverse analysis generally is conducted by employing the responses in either time or frequency domain [5–7]. As one type of inherent characteristics of a structure, mode shapes and their curvatures have been employed owing to their capability of reflecting local

* Corresponding author.
E-mail addresses: kzhou@mtu.edu (K. Zhou), jiong.tang@uconn.edu (J. Tang).

https://doi.org/10.1016/j.jsv.2021.116331
Received 30 November 2020; Received in revised form 3 June 2021; Accepted 29 June 2021
Available online 2 July 2021

structural property variation [8–10]. Most previous research efforts in this regard, however, have been conducted toward the deterministic case, i.e., the FE model is deterministic whereas all the information involved including measurements is also deterministic. In reality, the baseline finite element model to be updated is subject to numerical modeling error, and many parameters involved in the model are intrinsically uncertain due to manufacturing tolerance and measurement noise/error. An inverse analysis procedure that is deterministic cannot effectively address such uncertainties.

As can be seen, inverse analysis should be conducted in the probabilistic sense, i.e., treating model parameters to be updated as random variables with mean and variance. This can reveal the underlying properties of structures under uncertainties and variations. There have been some probabilistic approaches developed to investigate the parametric estimation in the presence of uncertainties. For example, Moaveni et al. [11] implemented sensitivity-based approach for damage identification, in which the uncertainty level that affects the identification result is quantified through analysis-of-variance (ANOVA) and meta-modeling. Khodaparast et al. [12] used kriging predictor to conduct interval model updating where irreducible uncertainty was considered. Bayesian inference naturally appears to be one of the most popular approaches, in which a probabilistic model is established to correct the prior beliefs based on the evidence [13]. It starts from characterizing the concerned model parameters in the form of probability density function (PDF) based upon the prior knowledge. This specific PDF is referred to as prior PDF or hypothesis in Bayes' rule. The actual response measurement is treated as evidence, and can be incorporated to update the prior PDF into the so called posterior PDF, based upon which the best model parameters can be identified. Bayesian inference not only can avoid the direct inversion for parameter estimation required in some sensitivity-based methods that may introduce some numerical issues, but also can directly incorporate various sources of uncertainties into model updating procedure [14]. Owing to its intrinsic advantages, there have been considerable successes in utilizing Bayesian inference to solve a variety of engineering problems [15–19]. Additionally, as the training scheme of meta-models, which are essentially implicit statistical regression models, is generally established upon Bayesian inference, exploring the potential closed-form of optimization objective function under Bayesian framework may benefit meta-model training efficiency [20].

It is worth noting that, while Bayesian inference can enable probabilistic FE inverse analysis under uncertainties, currently its application to complex structures is subject to certain limitations. One significant limitation lies in the huge computational cost of brute force Monte Carlo simulations of repeated finite element analyses. The computational cost will become intractable especially when the number of model parameters to be identified increases. Indeed, as the number of parameters to be identified increases, the search space dimension increases which requires a very large number of FE simulation runs in order to identify the updating result. The usual treatment to alleviate the computational cost is either to develop first principle-based order-reduction model [21] or resort to data-based surrogate model [22] to replace the original, large-scale finite element model. The first category of methods is inevitably subject to model truncation error due to order-reduction. Such error may become considerable when compared with the discrepancy between the actual measurement and finite element model prediction. In the second category of methods, it is difficult to rigorously determine the size of dataset needed. In certain cases, it is even difficult to decide how to select dataset from FE simulations to train/establish a surrogate model to accurately approximate the original FE model. On the other hand, improved sampling techniques, which may reduce the computational cost through reducing the number of FE simulation runs, have been extensively investigated. One popular approach is the Markov chain Monte Carlo (MCMC) method, which can be seamlessly integrated into Bayesian inference-based optimization [23–26]. It comprises a class of algorithms e.g., Metropolis-Hastings (MH) [27], Gibbs sampling (GS) [28] and importance sampling [29] to enable efficient sampling from an unknown target distribution/function. The constructed Markov chain hence is deemed as an equilibrium distribution of target distribution/function [30]. The number of samples in Markov chain is considerably smaller. Among these algorithms, MH-based MCMC is the most common method used in the application of FE model updating [27,31]. When MH-based MCMC method is applied, a proposal distribution is formulated to guide the sample generation over the entire parametric space. Generally, the variance of the proposal distribution is set as constant in the course of chain evolution.

The underlying idea of MCMC can lead to an accelerated approximation of target distribution. Here the target distribution essentially represents the actual objective surface in model updating. In this research, the actual objective surface is defined as the error surface between the FE prediction and the measurement with respect to the model parameter samples. It is worth noting that, in almost all practical situations, the number of sensors is limited and much smaller than the number of degrees of freedom (DOFs) in the structural model, and generally only the dynamic responses within the lower-order frequency range can be realistically measured. Therefore, the measurement acquired is incomplete. In many cases the inverse analysis-based model updating problem is underdetermined. Consequently, the objective surface may become very complex, exhibiting many local optima. In practice, a local optimum is a solution that is optimal (either maximal or minimal) within a neighboring set of candidate solutions. In this context, the optimum may appear as a local peak (or valley) as long as it is greater (or smaller) than the neighboring objective values. Moreover, different local optima should be well-separated over the entire parametric space. Conventional Bayesian model updating is performed with single MCMC, which is only capable of converging to one optimum. This optimum may very well be a local one. Therefore, it is critically important to find as many (local) optima as possible in actual scenarios, which allow one to further integrate additional information (e.g., additional measurements for validation) or empirical knowledge for the eventual decision making. This offers the flexibility in model parameter updating. Intuitively, through running single MCMC multiple times, we may collect their respective solutions as multiple local optima due to the random-walk nature of MCMC [32]. However, it cannot be guaranteed that the solution of each emulation run converges to a different local optimum. In other words, some solutions may be identical, which at least is not computationally effective. Additionally, the proposal distribution in MCMC usually has fixed variance which may further increase the chance of being trapped in local optimum. Several approaches have been attempted to address the issue of proposal distribution. For example, Liang et al. [33] proposed a Markov chain Monte Carlo method with adaptive proposal distribution for performance enhancement. Ji and Schmidler [34] formulated a mixture proposal distribution which can adapt to samples from multimodal target distribution, and demonstrated improved approximation. Recently, Lam et al. [35] developed a multiple parallel MCMC-based

Bayesian model updating approach to ensure the accuracy of updating results.

The objective of this research is to fundamentally address the challenges in computational inference using FE inverse analysis, i.e., underdetermined problem with complex objective surface. Specifically, we enhance the Bayesian inference-based inverse analysis framework with the integration of multiple parallel, interactive and adaptive Markov chains. We not only maintain the parallel scheme of Markov chains [35], but also enable all Markov chains to evolve in an interactive manner. The redundant Markov chains that yield the same local optima with others will be suspended in order to alleviate the computational cost. Meanwhile, an automatic analysis procedure is employed to adaptively determine the number of Markov chains and related initial parameters to be executed. As will be demonstrated in this research, these strategies can take full advantage of the characteristics of dynamic responses utilized in FE inverse analysis such as incomplete modal response information to unleash the potential of physics informed statistical inference. The rest of this paper is organized as follows. In Section 2, the general formulation of finite element (FE) inverse analysis using incomplete modal response information is outlined first, followed by an overview of traditional Bayesian inference-based inverse analysis integrated with single Markov Chain which serves as the baseline. Subsequently, the enhanced framework built upon multiple parallel, interactive and adaptive Markov chains is then presented. Section 3 provides implementation details and systematic case studies on a benchmark structure to demonstrate the proposed methodology and illustrate the performance improvement. Section 4 gives the concluding remarks.

2. FE inverse analysis with enhanced bayesian framework: algorithm development

This section presents the formulation of FE inverse analysis with enhanced Bayesian framework. We start from the problem formulation of FE inverse analysis using (incomplete) modal response information. It is followed by the outline of conventional Bayesian updating. The new framework is then established where the enhancement through incorporating multiple Markov chains is highlighted.

2.1. Problem formulation of FE inverse analysis using incomplete modal response information

Finite element (FE) inverse analysis is a widely used procedure to identify model parameters or their updates based on measurement or desired/target outcome. In structural fault identification, the input is the response of structure being monitored, and the output is the damage index vector (i.e., location and severity of local property change). In design optimization, the input is the desired/target response, and the output is the modification of design parameters. And in model updating to ensure the modeling validity, the input is the measurement of actual structural response under controlled excitation, and the output is the FE model parameters. In sampling based inverse analysis, the response prediction from a baseline FE model under given sampled parameters is compared with the measurement or target to facilitate the identification. The FE-based dynamic equation of motion can be expressed as

$$\mathbf{M}\ddot{\mathbf{x}} + \mathbf{C}\dot{\mathbf{x}} + \mathbf{K}\mathbf{x} = \mathbf{F} \tag{1}$$

where **M, C**, and **K** are the mass, damping, and stiffness matrices, respectively. We assume the structure has N DOFs. All the system matrices are of dimension $N \times N$. $\mathbf{x}$ is the N-dimensional displacement vector. Let the structure be subject to light and proportional damping. The damping matrix thus is dependent on the mass and stiffness matrices. Without loss of generality, in what follows we are only concerned about the inverse analysis of stiffness matrix. The inverse analysis of both the mass and stiffness matrices can be formulated similarly.

In practice, owing to the high dimensionality of FE model, it is impossible to identify all elemental stiffness and mass matrices. Commonly, we assume that variations of model parameters (i.e., parameters to be identified) only occur at n ($n \ll N$) elements or segments in the FE model. Let $\mathbf{K}_i$ denote the nominal stiffness matrix of the i th segment in the original, baseline FE model. The global stiffness matrix that is subject to variation thus can be expressed as [36]

$$\widehat{\mathbf{K}} = \sum_{i=1}^{n} \mathbf{K}_i(1-\alpha_i) \tag{2}$$

where α_i indicates the stiffness variation coefficient of the i th segment. The summation shown in Eq. (2) represents the usual direct sum in FE modeling. In this research, we let α_i fall into $[0, \quad 1]$. The coefficient vector, $\boldsymbol{\alpha} = [\alpha_1, \alpha_2 \ldots \alpha_i \ldots \alpha_n]$, represents the unknown stiffness variations to be identified. The aforementioned formulation can be directly applied to fault identification, design optimization, and model updating. In those applications, $\boldsymbol{\alpha} = [\alpha_1, \alpha_2 \ldots \alpha_i \ldots \alpha_n]$ represent, respectively, the unknown stiffness reductions caused by fault, the stiffness changes necessary to facilitate target response; or the stiffness parameters to be updated to match the experimental measurement for model updating.

The stochastic FE model of the actual structure, that is perturbed by the unknown parameters to be identified, thus becomes

$$\widehat{\mathbf{M}}\ddot{\mathbf{x}} + \widehat{\mathbf{C}}(\boldsymbol{\alpha})\dot{\mathbf{x}} + \widehat{\mathbf{K}}(\boldsymbol{\alpha})\mathbf{x} = \mathbf{F} \tag{3}$$

Here $\widehat{\mathbf{M}} = \mathbf{M}$ which remains invariant, and the stiffness and damping matrices are affected by $\boldsymbol{\alpha}$. The modal information of this system is governed by the following eigenvalue problem,

$$\left[\widehat{\mathbf{K}}(\boldsymbol{\alpha}) - \left(2\pi\widehat{\omega}_i\right)^2 \widehat{\mathbf{M}}(\boldsymbol{\alpha})\right]\widehat{\psi}_i = \mathbf{0} \tag{4}$$

The i th natural frequency and the corresponding mode shape are denoted as, $\widehat{\omega}_i$ and $\widehat{\psi}_i$, respectively. They are both functions of $\boldsymbol{\alpha}$.

In inverse analysis practice, usually the first q ($q \ll N$) lower-order natural frequencies and mode shapes can be acquired or experimentally extracted. For example, in fault identification and model updating, in actual data acquisition, only a small number of s ($s \ll N$) sensors can be employed at the corresponding DOFs for measurement [10]. The modal information acquired thus is incomplete and limited. For notation convenience, we let $(\overline{\omega}_{1\times q},\overline{\psi}_{s\times q})$ denote the measurement information consisting of first q natural frequencies and an $s \times q$ matrix of the collection of corresponding mode shape vectors. Hereafter the subscripts of these variables indicate their dimensions. In each mode shape vector, only the modal amplitudes at s DOFs are measured. Similarly, we let $(\widehat{\omega}_{1\times q},\widehat{\psi}_{s\times q})$ denote the information simulated/predicted from the FE model (Eq. (4)). Our goal is to identify the set of uncertain parameters, $\boldsymbol{\alpha}$, such that the difference between $(\overline{\omega}_{1\times q},\overline{\psi}_{s\times q})$ and $(\widehat{\omega}_{1\times q},\widehat{\psi}_{s\times q})$ is minimized. To properly quantify such difference, the direct matching of the numerical and experimental modes is required. In actual practice, certain modes predicted in the numerical simulation may not appear in experimental measurement. The mode veering may also occur due to the varying model parameters especially when the associated natural frequencies are very close [37]. The direct mode matching using the mode order hence becomes ineffective. The potential methods to address this challenge include the Modal Assurance Criteria (MAC) and model reduction [38,39]. MAC is a metric to correlate the modes through comparing their mode shape patterns. Owing to its conceptual simplicity and implementation convenience, we adopt the MAC-based mode matching procedure in this study. While the mathematical details will be provided subsequently, here we generically express the differences of natural frequencies and mode shapes as $\kappa(\overline{\omega}_{1\times q}, \widehat{\omega}_{1\times q}(\boldsymbol{\alpha}))$ and $\upsilon(\overline{\psi}_{s\times q}, \widehat{\psi}_{s\times q}(\boldsymbol{\alpha}))$, respectively, which are to be minimized. As mentioned, in this research the methodology to be developed will incorporate various uncertainties and measurement noise. Therefore, $\kappa(\overline{\omega}_{1\times q}, \widehat{\omega}_{1\times q}(\boldsymbol{\alpha}))$ and $\upsilon(\overline{\psi}_{s\times q}, \widehat{\psi}_{s\times q}(\boldsymbol{\alpha}))$ are no longer deterministic. They are instead probabilistic. The model parameters $\boldsymbol{\alpha}$ will be identified in a probabilistic manner accordingly.

2.2. Conventional Bayesian inverse analysis with MCMC

2.2.1. Bayesian inference

The objective of this research is to develop a new framework to identify or update, probabilistically, the FE model based on measurement or target information. In the model updating practice, the underlying idea of Bayesian inference is to update the probability of hypothesis as more measurements become available, which fits the research objective. It is well known that Bayesian inference is established upon the Bayes' rule which is fully represented as [13]

$$p(\boldsymbol{\theta}|\boldsymbol{\Omega}) = \frac{p(\boldsymbol{\Omega}|\boldsymbol{\theta})p(\boldsymbol{\theta})}{\int p(\boldsymbol{\Omega}|\boldsymbol{\theta})p(\boldsymbol{\theta})d\boldsymbol{\theta}} \tag{5}$$

In the context of FE inverse analysis, the hypothesis $\boldsymbol{\theta}$is interpreted as the vector of model parameters (i.e.,$\boldsymbol{\alpha}$in Eq. (2)) to be updated. The measurement data, $\boldsymbol{\Omega}$, is the modal information difference (between model prediction and actual measurement or target information), i.e., $\kappa(\overline{\omega}_{1\times q}, \widehat{\omega}_{1\times q}(\boldsymbol{\alpha}))$ and $\upsilon(\overline{\psi}_{s\times q}, \widehat{\psi}_{s\times q}(\boldsymbol{\alpha}))$. Hereafter to simplify the notations we refer to the differences of natural frequencies and mode shapes as $\kappa(\boldsymbol{\alpha})$ and $\upsilon(\boldsymbol{\alpha})$. We thus re-write the above equation as

$$p(\boldsymbol{\alpha}|\kappa(\boldsymbol{\alpha}),\upsilon(\boldsymbol{\alpha})) = \frac{p(\kappa(\boldsymbol{\alpha}),\upsilon(\boldsymbol{\alpha})|\boldsymbol{\alpha})p(\boldsymbol{\alpha})}{\int p(\kappa(\boldsymbol{\alpha}),\upsilon(\boldsymbol{\alpha})|\boldsymbol{\alpha})p(\boldsymbol{\alpha})d\boldsymbol{\alpha}} \tag{6}$$

The prior PDF $p(\boldsymbol{\alpha})$ is an arbitrary distribution of $\boldsymbol{\alpha}$ initially created based on prior knowledge. Without explicit understanding of the target problem, this term can be simply defined as a standard statistical distribution, such as normal or uniform distribution. The likelihood PDF $p(\kappa(\boldsymbol{\alpha}),\upsilon(\boldsymbol{\alpha})|\boldsymbol{\alpha})$ aims at probabilistically assessing the agreement between the measurement/target and the corresponding modal information prediction from the model. The posterior PDF $p(\boldsymbol{\alpha}|\kappa(\boldsymbol{\alpha}),\upsilon(\boldsymbol{\alpha}))$ is the resultant distribution of $\boldsymbol{\alpha}$conditioned on the prior PDF and the measurement. Since the marginal likelihood in the denominator essentially is a normalization constant, the posterior PDF is proportional to the numerator, i.e., $p(\boldsymbol{\alpha}|\kappa(\boldsymbol{\alpha}),\upsilon(\boldsymbol{\alpha}))\infty p(\kappa(\boldsymbol{\alpha}),\upsilon(\boldsymbol{\alpha})|\boldsymbol{\alpha})p(\boldsymbol{\alpha})$. It is worth noting that the posterior PDF here is considered as the optimization objective to guide the model updating/optimization process, in which the best parametric combination, $\widetilde{\alpha}$, can be identified with the highest $p(\widetilde{\alpha}|\kappa(\widetilde{\alpha}),\upsilon(\widetilde{\alpha}))$.

To implement the Bayesian inference, we will need to build the probabilistic relationship between the measurement/target and the corresponding modal information prediction in the presence of uncertainties. In this research, measurement/target and modeling errors are considered as Gaussian noise. The likelihood PDF that takes into account the effect of these errors thus is subject to a multivariate normal distribution. The specific formulation of likelihood PDF is dependent on the explicit forms of $\kappa(\boldsymbol{\alpha})$ and $\upsilon(\boldsymbol{\alpha})$, which will be discussed later.

2.2.2. Integration of MCMC for expedited optimization

In order to identify the model parameters, Bayesian inference-based optimization will be conducted which requires Monte Carlo simulation with repeated FE analyses. For a practical structure, each FE analysis run will take certain computational cost. A brute force Monte Carlo simulation would be computationally prohibitive, as a very large number of parametric combinations need to be substituted into this procedure to construct a credible posterior PDF. The computational issue will be further compounded when high-dimensional parametric set, i.e., large n in Eq. (2), is involved. A common solution is to adopt Markov chain Monte Carlo (MCMC) to replace the conventional Monte Carlo to facilitate efficient model updating analysis under uncertainties.

The fundamental idea of MCMC is that it can generate a stationary chain with a significantly reduced number of model parameter

samples that are used to approximate the target distribution [24,30,40]. The approximated distribution is capable of interpreting the best parametric combination to be identified in a probabilistic sense. There are several classes of algorithms that can be utilized to execute MCMC, in which the Metropolis-Hastings (MH) and Gibbs samplings are two representative ones. Gibbs sampling or a Gibbs sampler can allow the identification of multiple sets of parameters. Specifically, the conditional posterior PDFs of the parameters of interest can be updated iteratively [28,41]. Generally, Gibbs and MH sampling algorithms have different strengths. In some cases, Gibbs sampling may require MH algorithm when dealing with complex conditional targets, while MH proposals may be built to approximate the full conditionals (Gibbs). Leveraging the combination of both Gibbs and MH samplings, the model updating performance may indeed be improved [32]. Since the specific emphasis of this research lies in the computational enhancement, i.e., integrating multiple parallel and interactive Markov chains, we adopt the standard architecture of MH MCMC for demonstration. The pseudo code of the MH MCMC is shown below.

Pesudo code of Metropolis-Hastings (MH) MCMC

With $\boldsymbol{\alpha}_t^*$ at time t, the aim is to generate the next chain value $\boldsymbol{\alpha}_{t+1}^*$.

1. Proposal step: Sample "Candidate" $\boldsymbol{z}$ from the proposal distribution $\mathbf{Z} \sim q(\mathbf{z}|\boldsymbol{\alpha}_t^*)$. Proposal distribution usually is selected as a symmetrical distribution, e.g., normal distribution.

2. Acceptance step: With probability $\beta(\mathbf{Z},\boldsymbol{\alpha}_t^*) = \min\left(1, \frac{p(\boldsymbol{\alpha}_t^*|\kappa(\boldsymbol{\alpha}_t^*),\upsilon(\boldsymbol{\alpha}_t^*))q(\mathbf{Z}|\boldsymbol{\alpha}_t^*)}{p(\mathbf{Z}|\kappa(\mathbf{Z}),\upsilon(\mathbf{Z}))q(\boldsymbol{\alpha}_t^*|\mathbf{Z})}\right)$. Due to the symmetry of proposal distribution, $q(\mathbf{Z}|\boldsymbol{\alpha}_t^*) = q(\boldsymbol{\alpha}_t^*|\mathbf{Z})$.

Generate μ from a uniform (0, 1) distribution:
if $\beta(\mathbf{Z},\boldsymbol{\alpha}_t^*) > \mu$, we set $\boldsymbol{\alpha}_{t+1}^* = \mathbf{Z}$(i.e., acceptance)
else $\boldsymbol{\alpha}_{t+1}^* = \boldsymbol{\alpha}_t^*$ (i.e., rejection).

Note: $q(\mathbf{z}|\boldsymbol{\alpha}_t^*)$is the proposal distribution of $\boldsymbol{z}$ depending on the deterministic parameter $\boldsymbol{\alpha}_t^*$.

In MH MCMC, 'Metropolis criterion' is strictly followed to determine whether the newly generated sample is retained or discarded. Through executing the analysis of MCMC, we can obtain the Markov chain containing all accepted model parameter samples and their posterior probability values. The reduced number of samples in MCMC leads to significant reduction of computational cost. The accepted model parameter samples in Markov chain can be further used to estimate/approximate the posterior PDF for probabilistic parameter updating. The conventional single MCMC-based Bayesian inverse analysis framework introduced in this Section is shown in Fig. 1.

2.3. Enhanced Bayesian inverse analysis framework with integration of multiple parallel, interactive and adaptive Markov chains

In inverse analysis using vibration response, generally only the lower-order modal information is used (e.g., realistically measured in fault identification and model updating). Moreover, as the number of sensors is limited, the mode shape information is incomplete. When the number of model parameters to be updated is large, the inverse problem is oftentimes underdetermined. Moreover, the objective surface in inverse identification oriented optimization is very complex, exhibiting many local optima. Conventional Bayesian inverse analysis performed with single MCMC which is outlined in the Section 2.2 is only capable of converging to one optimum which may not likely be the best result. To tackle this challenge, in what follows we develop the key component in the enhanced inverse analysis framework, i.e., the parallel, interactive and adaptive Markov chains, which aims at adequately approximating the target distribution over the entire space of model parameters to be identified/updated.

We first want to ensure capturing as many local optima as possible, and thus adopt a parallel scheme of Markov chains, similar to what's suggested in literature [35]. Generally, to increase updating accuracy, the number of Markov chains, i.e., m, is suggested to be large especially for cases with complicated objective surface to be characterized. The m resulting Markov chains can be utilized to identify the probabilistic solutions. Building upon this, we include an adaptive scheme for varying proposal distribution width in order to improve the performance of MCMC [33]. Specifically, we assign a small width γ for proposal distribution in the beginning, since

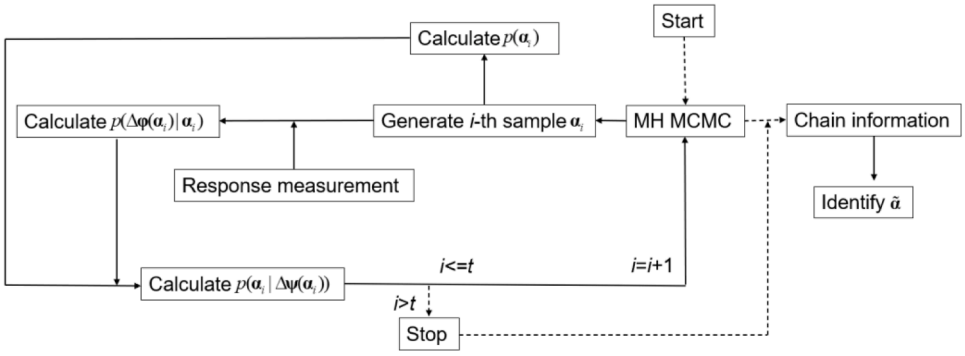

Fig. 1. Conventional Bayesian inverse analysis.

different Markov chains are designated to search parameters at respective local areas. It is noted that the width here is controlled by the distribution standard deviation defined. A small width thus benefits the dense search process. During the MCMC evolution, the distribution width is adaptively tuned with respect to the chain status in order to avoid the trapping by local optima. The pseudo code of such adaptive width variation rule is given below.

Pesudo code of adaptive proposal distribution width variation

```
Set a small width for the proposal PDF γ
MCMC evolution iteration:
…..
Counting the consecutive rejection steps
If the number of the consecutive rejection steps fall in the range [q1, q2]
Set a larger width of proposal PDF γ1
If the number of the consecutive rejection steps fall in the range [q2, q3]
Set a larger with of proposal PDF γ2
If the current sample is accepted,
The original small width of proposal PDF γis restored.
……
```

Note: $\gamma < \gamma_1 < \gamma_2 < ...\gamma_p$, and $q_1 < q_2 < ...q_{p+1}$

There are, however, remaining issues. The first issue is that the selection of m Markov chains. In earlier investigations, m is manually selected according to the configuration of computational platform, such as the number of processors [35]. In particular, the initial parameters of m chains are either randomly generated based upon a pre-specified statistical distribution or grid-discretized to uniformly cover the entire parametric space. These procedures may not yield optimal initial parameters, which thus slows down the convergence of Markov chains. The second issue is that, while these m Markov chains evolve independently in parallel, it is not guaranteed that all of them will finally converge to m different, well-separated local optima. Additionally, if some Markov chains already converge to the same local optima and still are allowed for continuous evolution, computational resource will be occupied unnecessarily. In this research we aim at developing a new Bayesian inverse analysis framework using incomplete modal information. While the mathematical details will be presented in the next section, the treatments to address the aforementioned issues are introduced as follows.

We establish a sequential procedure for the m parallel Markov chains (Fig. 2). We construct a uniform distribution covering the entire parametric space, based on which we randomly generate w model parameter samples. Without prior knowledge, we perform the Monte Carlo simulation to calculate the objective values (i.e., posterior probability values) of these parameter samples following Eq. (6). We then sort the objective values and find the r best model parameter samples with higher objective values. Following this, we utilize the K-means clustering analysis to take advantage of the sorted samples. The K-means clustering analysis can partition data into different clusters with the nearest mean [42]. The clustering process is implemented by iteratively updating the means of obtained clusters until the convergence criterion is met. The distance between two model parameter samples is represented by the Euclidean distance of the associated spatial coordinates [43]. We will implement K-means clustering analysis based on w model parameter samples. The K-means clustering analysis is an important element of this proposed approach as it can automatically identify the

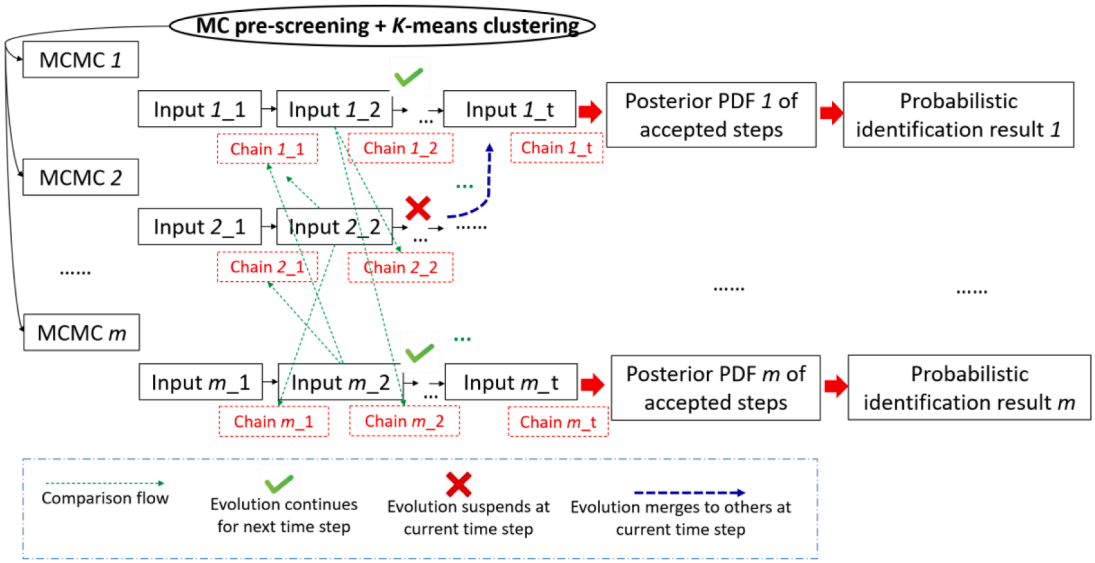

Fig. 2. Schematic illustration of integration of *parallel, interactive* and *adaptive* Markov chains.

optimal locations to start the MCMC evolution. As a result, the model updating performance, i.e., analysis convergence and diversity (i.e., multiple local optima detection capability), can be significantly improved. It is worth noting that the number of clusters or the number of initial chains is a hyperparameter of the *K*-means clustering analysis, which is to be optimally determined. To balance the trade-off between the solution search efficiency and on-demand computational resources, we set a proper range, i.e., [5, 20] for the cluster number. The number of clusters starts to increase from the lower bound, i.e., 5, with a distance constraint that the distance between any two clusters should exceed the minimal distance specified. The maximum number of clusters m ($m \leq r$and $m \in [5,\ 20]$) can be determined once the distance constraint is marginally satisfied. Because such distance constraint essentially is related to the Silhouette coefficient that is a typical clustering performance metric [44], we can simply use it to direct the automatic selection of cluster number for *K*-means clustering analysis. We further consider m centers of m generated clusters as initial model parameters to execute the m parallel Markov chain evolutions.

To address the second issue in the parallel Markov chains, we integrate a procedure for the merge check of Markov chains during evolutions. At each time step, currently accepted model parameter sample of one certain MCMC will be compared with all accepted model parameter samples archived in other Markov chains. When it occurs that the Euclidean distance of two compared model parameter samples is smaller than a threshold, one MCMC is suspended and will not continue to evolve in the next time step. This allows the interaction of all Markov chains. The final number of the resulting Markov chains is z, where $z \leq m$. Correspondingly, z solutions, i.e., z unique local optima, will be identified through the chain information obtained. There indeed have been multiple criteria suggested for terminating the MCMC evolution. One popular criterion is dependent on the convergence examination, in which the auto-correlation degree of Markov chain is iteratively assessed as the evolution proceeds [45]. A threshold of auto-correlation degree will be prescribed to decide whether the evolution can be terminated. Another criterion is to directly assign a maximum iteration number for MCMC evolution [10]. In this research, for the sake of illustration we adopt the latter one. When a pre-specified iteration number, i.e., t of Markov chain, is reached, the whole process will be terminated. The earlier termination also allows to ensure the computational efficiency when the specified number of consecutive rejected steps, i.e., u is reached. The eventually survived Markov chains can offer the information to extract the probabilistic updating results.

This enhanced framework is schematically illustrated in Fig. 2. To maintain the stationary property of MCMC, first a few accepted samples in the transition phase, the so-called burn-in period, need to be scrapped [46]. Hence, the burn-in length ratio κshould be defined in the analysis.

3. New framework implementation details and case demonstrations

This section presents the mathematical details of the enhanced Bayesian inverse analysis framework through implementing case investigations. In order to validate the effectiveness and generality of the new approach, we practice the algorithmic implementation to two different, representative scenarios, i.e., identifying boundary conditions of a dome structure and updating material properties of a plate structure with high FE mesh density. In both cases, limited and incomplete modal information will be used to facilitate inverse analysis. In this research we use simulated data in lieu of experimental data to facilitate inverse analysis for algorithm investigation. This allows interested readers to reproduce the results for examination. Moreover, since the 'ground truth' is known in the simulated cases, the effectiveness and accuracy of the new framework can be thoroughly investigated, especially in the presence of many local optima in Bayesian inference based optimization.

3.1. Implementation scenario 1: boundary condition updating of a dome structure

3.1.1. Inverse analysis problem setup

We choose the parametric identification of a dome-type structure as the first implementation scenario, as it is representative of many civil infrastructures. The configuration and geometric parameters are shown in Fig. 3. It is made of homogeneous material with Young's modulus 2.06×10^{11}Pa, mass density 7.85×10^{3}kg $/m^{3}$, and Poisson's ratio 0.3. The finite element model of this structure is built with the beam element, containing a total 108 of nodes (each node with 3 translational DOFs). The cross section of beam element is rectangular with area $0.0168m^{2}$(cross section length and width: 0.21 m and 0.08 m, respectively). In this dome structure, 18 nodes at

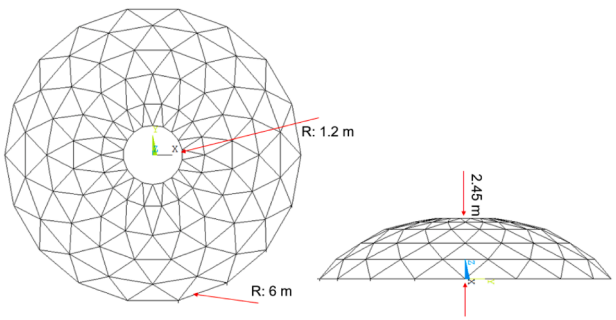

Fig. 3. The geometry of the dome structure. Outer radius: 6 m; inner radius: 1.2 m; height: 2.45 m.

the bottom layer are imposed with boundary conditions, i.e., being fixed to ground. We assume in this case 14 out of 18 nodes are indeed completely fixed (i.e., no displacement at all 3 directions). And we assume the other 4 nodes are not fixed ideally, with stiffness parameters to be identified based on simulated measurement information. To a large extent, updating boundary conditions essentially is to calibrate the stiffness at boundary DOFs. To facilitate such analysis, we employ 3 spring elements that are aligned with 3 principal directions of each node and connected with the ground to emulate the boundary conditions (Fig. 4). If a boundary DOF is completely fixed, the corresponding spring stiffness is theoretically infinity. On the other hand, if a boundary DOF is not completely fixed, a finite spring stiffness value will need to be identified.

Without loss of generality, the stiffness values of 3 springs connected to the same node are assumed to be the same. Therefore, in this case analysis we have 4 spring stiffness values to be updated, i.e., the total number of unknowns to be updated is 4. Before conducting the model updating analysis, we first estimate the order of magnitude of such spring elements. It is found that once we increase the boundary stiffness values of the aforementioned 4 nodes to $1 \times 10^{24}\mathrm{N/m}$, the natural frequencies of the dome structure approach those of the dome with all 18 nodes fixed. Therefore, we can consider $1 \times 10^{24}\mathrm{N/m}$ being the stiffness value corresponding to the fixed boundary condition. As such, we define the entire search interval as $[0, 1 \times 10^{24}]\mathrm{N/m}$. This can ensure the detection of the response with respect to the boundary condition change. For this particular case, we treat the upper bound of stiffness (i.e., $1 \times 10^{24}\mathrm{N/m}$) as the nominal value, and assume the actual spring stiffness reductions due to non-ideal boundary conditions at these 4 nodes are given as $\Delta\mathbf{K} = [0.7 \times 10^{24}, 0.6 \times 10^{24}, 0.1 \times 10^{24}, 0.9 \times 10^{24}]\mathrm{N/m}$. Therefore, the actual stiffness reduction coefficients to be identified are $\overline{\alpha} = [0.7, 0.6, 0.1, 0.9]$. We define the prior PDF of model parameters, i.e., 4 spring stiffness reduction coefficients, as a multivariate uniform distribution with range [0, 1]. In what follows we use simulated data in lieu of experimental data to conduct the model updating practice. Since the 'ground truth', i.e., the true boundary condition, is known in this case study, we will be able to fully demonstrate the algorithmic improvement.

Since we are subject to incomplete modal information measurement, we assume only the first two natural frequencies and the associated mode shapes are available for model updating. Moreover, we assume only 4 sensors (uniaxial accelerometers) installed along the z-direction at 4 nodes indicated in Fig. 5 are employed. Therefore, only the amplitudes of the mode shapes at these DOFs are measurable. For demonstration, the 1st z-bending mode shape of the dome structure is also shown in Fig. 5. Throughout model updating, the measurement information will be compared with model prediction iteratively/continuously. Here we utilize the mode assurance criterion (MAC) to assess the difference between the mode shape prediction and the measurement [47]. Given two mode shapes for comparison, MAC directly converts the vector difference into a scalar. As a result, the influence of mode shape and natural frequencies can be equivalently incorporated into the formulation of the posterior PDF.

Recall that in Section 2.1 the differences of natural frequencies and mode shapes are generically expressed as $\kappa(\boldsymbol{\alpha})$ and $\upsilon(\boldsymbol{\alpha})$ where $\boldsymbol{\alpha}$ is the vector of model parameters to be updated. We now let

$$\kappa(\boldsymbol{\alpha}) = \sum_{i=1}^{q} \frac{\left|\widehat{\omega}_i - \overline{\omega}_i\right|}{\overline{\omega}_i}, \tag{7a}$$

$$\upsilon(\boldsymbol{\alpha}) == \sum_{i=1}^{q} (1 - \gamma_i) \tag{7b}$$

where γ_i is MAC that is defined as $\gamma_i = \frac{|\widehat{\psi}_i^T \overline{\psi}_i|^2}{(\widehat{\psi}_i^T \widehat{\psi}_i)(\overline{\psi}_i^T \overline{\psi}_i)}$ [47]. Hereafter the hat notation indicates variable obtained through model prediction, and the bar notation indicates variable obtained from measurement. As simulated data are used in lieu of actual measurement, $\overline{\omega}_i$ and $\overline{\psi}_i$ are obtained numerically from the baseline model with $\overline{\alpha} = [0.7, 0.6, 0.1, 0.9]$.

We further derive the likelihood PDFs of both $\kappa(\boldsymbol{\alpha})$ and $\upsilon(\boldsymbol{\alpha})$with the normal distribution given as

$$p(\kappa(\boldsymbol{\alpha})|\boldsymbol{\alpha}) = \prod_{i=1}^{q} \exp\left(\frac{-\left(\left|\omega_i - \overline{\omega}_i\right|\right)^2}{2\left(\eta_i \overline{\omega}_i\right)^2}\right), \tag{8a}$$

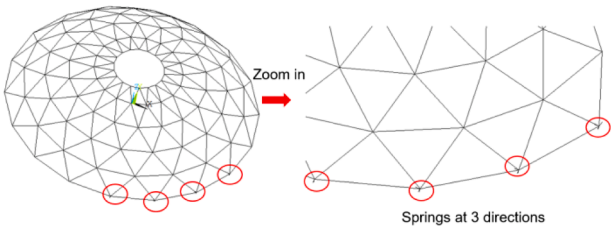

Fig. 4. Boudary condtions (i.e., 4 spring stiffness values) of the dome structure to be updated.

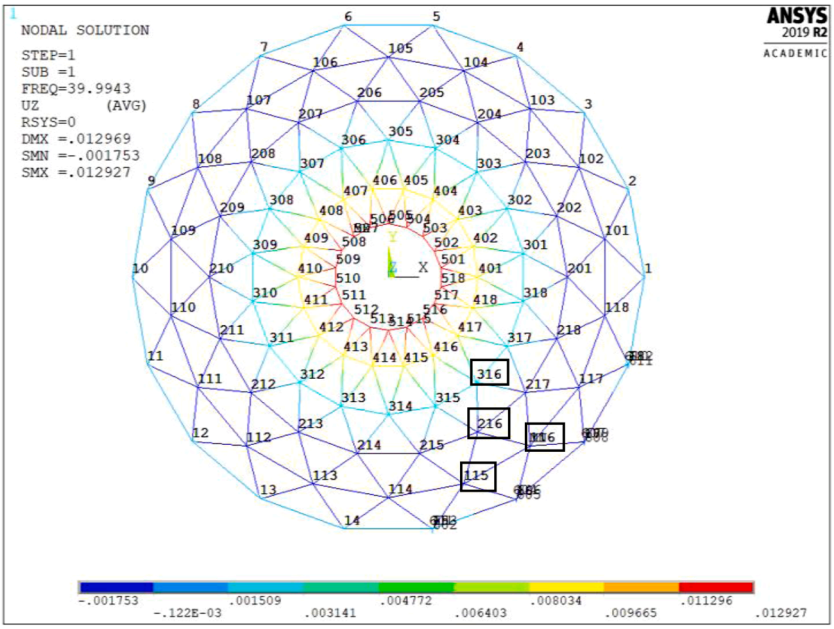

Fig. 5. 1st z-bending mode shape of the dome structure attached with 4 sensors (locations: node 115, 215, 216 and 316).

$$p(\upsilon(\boldsymbol{\alpha})|\boldsymbol{\alpha}) = \prod_{i=1}^{q} \exp\left(\frac{-(1-\gamma_i)^2}{2(\eta_i)^2}\right) \tag{8b}$$

A very important aspect of such model updating problem is the measurement noise, as actual measurement is always subject to noise effect. It is worth emphasizing that the above likelihood PDFs take into account the measurement noise through incorporating the variability level, i.e., η_i. The values of η_i are generally decided based on the noise level of experimental measurements. Previous literature has reported that the values of η_i can be estimated from the convergence of the statistics of the measured data, i.e., identified modal parameters. To allow unbiased estimation, usually a large number of repetitive measurements collected in the structure are needed [48]. These values indeed are case specific, depending on the structure investigated, data acquisition equipment resolution, sensor locations, ambient noise and mode order/frequency range of interest. In literature, the variability of measured natural frequencies generally falls into the range [0.5%, 3%] [27,48–50]. It should be noted that modeling error could be more significant than measurement noise in practical scenarios [25]. To adequately take into account all the uncertainties for the posterior PDF characterization, relatively large values of η_i are suggested. Therefore, in this research η_i are chosen as 0.08 (i.e., 8%) for both the natural frequencies and MACs to take into account the noise/uncertainties. As mentioned, η_i indeed can be updated in the form of conditional posterior PDF via the Gibbs sampling. Since the specific emphasis of this research lies in the computational inference algorithm development, for illustration purpose we decide to utilize the standard MH MCMC, in which $\eta_i$is appropriately selected as a constant

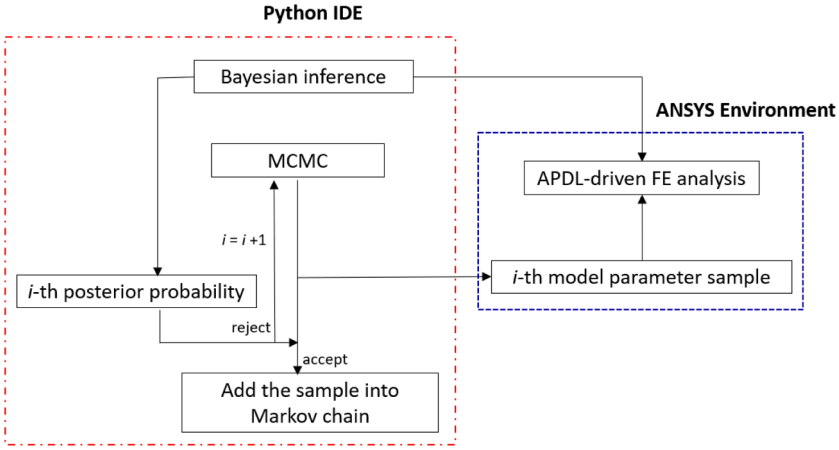

Fig. 6. Analysis flowchart that enables the interaction between ANSYS and Python.

based upon the literature [25,27,48–50]. We assume the PDFs of natural frequencies and mode shapes are statistically independent. The final likelihood thus can be written as

$$p(\kappa(\boldsymbol{\alpha}), \upsilon(\boldsymbol{\alpha})|\boldsymbol{\alpha}) = \prod_{i=1}^{q} \exp\left(\frac{-\left(\left|\widehat{\omega}_i - \overline{\omega}_i\right|\right)^2}{2\left(\eta_i \overline{\omega}_i\right)^2} + \frac{-(1-\gamma_i)^2}{2(\eta_i)^2} \right) \tag{9}$$

Substituting Eq. (9) into Eq. (6) yields the closed-form of the posterior PDF.

In this research, we establish the probabilistic updating framework using Python. We leverage the efficient solver of ANSYS [51] for finite element simulations, and incorporate it into the framework. APDL script is employed to direct the ANSYS analysis in the backstage. The interface between python IDE and ANSYS environment is built to facilitate the updating process. The framework developed is completely automated, and the entire Markov chain will be eventually produced through FE analysis iterations. For illustration, Fig. 6 shows the architecture of conventional Bayesian inverse analysis, indicating how the interaction between Python IDE and ANSYS environment takes place. This analysis architecture can be further extended to suit the enhanced updating framework with multiple Markov chains. The APDL pseudo code for finite element analysis under certain model parameter sample is given in Appendix for interested readers to reproduce the analysis result. In the current algorithm setup, aiming at identifying as many local optima as possible, we apply different chains, which will to certain extent increase the computational cost. Intuitively, parallel computing appears to be promising. However, generally it is applicable only when all the Markov chains evolve independently. In our

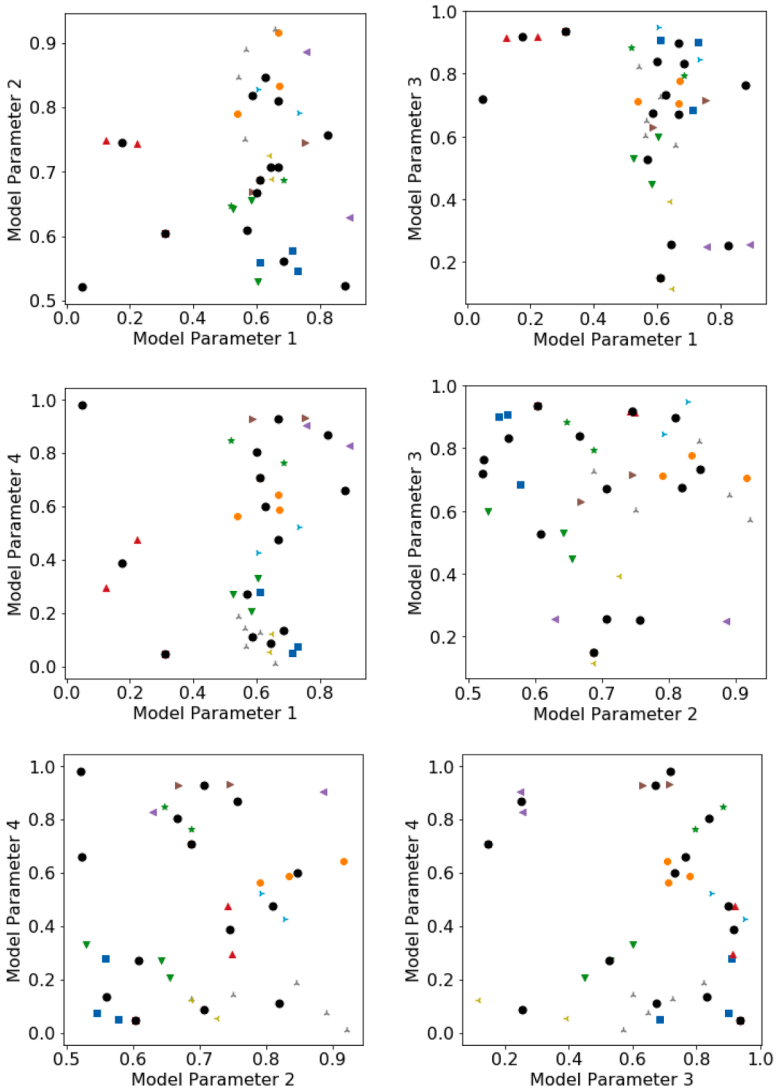

Fig. 7. Initial model parameter samples using *K*-means clustering analysis based upon pre-screened ranked model parameter samples from Monte Carlo simulation. (Circles denote the centers of clusters; other shapes denote the clusters.).

study, another important feature of the proposed approach is the frequent and simultaneous interaction of different chains over entire evolution, which poses a challenge for direct implementation of parallel computing. The fundamental reason is that the current approach resorts to the in-memory computation. The memory allocated at different python IDE environments is independent, which limits its parallel execution. Nevertheless, the proposed approach has the potential to accommodate parallel computing scheme. A feasible idea is to write the chain information from the memory into the intermediate files that can be shared and assessed by all chains during evolution. This can facilitate the parallel computing, and is subject to future research.

3.1.2. Inverse analysis practice using incomplete modal information

3.1.2.1. Direct parametric estimation with MCMC evolution. Following the procedures outlined in the Section 2.3, we first formulate a multivariate uniform distribution with bound [0, 1] to facilitate the Latin hypercube sampling [46] of 1000 (i.e., $w = 1000$) model parameter samples. The posterior probability values of these samples can be directly calculated using Monte Carlo simulation. We then screen 50 out of these 1000 samples (i.e., $r = 50$) with higher posterior probability values. With a pre-specified distance threshold, i.e., $\varepsilon_C = 0.23$, *K*-means clustering analysis is carried out to partition 50 pre-screened samples into 14 clusters. Each cluster is fully differentiated by its center information. The spatial coordinates of these centers are considered as the initial model parameters of respective 14 Markov chains to be executed.

Fig. 7 gives the 2-D cluster information yielded by *K*-means clustering analysis. The details of the operating variables can be found in Table 1. 14 Markov chains progressively evolve upon the initial parameters. Eventually, 6 Markov chains among them survive, and the rest of 8 merge to others. From the aspect of computational efficiency, we summarize the status of Markov chains as shown in Fig. 8. In each iteration, the major computational cost is spent in FE analysis, which takes around 2–3 s on a desktop computer with Intel CPU E5-2640 @2.40 GHz (2 processors). The overall computational cost therefore can be estimated in terms of the numbers of iterations for both merged and survived Markov chains (Fig. 8).

Recall the pseudo code of MH MCMC shown in Section 2.2.2. An important procedure, i.e., sample acceptance in MCMC, collects the 'useful' samples to approximate the target distribution in a statistical manner. The complete sample acceptance history can be represented by the resulting Markov chain. The trends of posterior probability values in survived Markov chains are presented in Fig. 9. It is worth noting here one Markov time step in the horizontal axis denotes one accepted sample. For notation convenience, each survived Markov chain can be deemed as one solution. One may notice that the index of Markov time step does not start from 1 because of the removal of 'burn-in' period as mentioned before. The maximum iteration number of MCMC is specified as 2000 (Table 1). The numbers of accepted time steps vary with respect to the Markov chain, which may be due to the different input-output relations around different local optima. Unlike general optimization methods, the objective value in this framework does not monotonically increase as process proceeds. This observation is directly due to the Metropolis criterion which takes place in the acceptance step (please refer to the MH MCMC pseudo code in Section 2.2.2). The random number generated for comparison will oscillate the objective values of accepted samples, which to certain extent can alleviate the trap of local optima. The maximum objective value is 1 as the posterior PDF is normalized. It is observed that the highest objective values of all solutions are relatively large. The values in Solutions 3, 4 and 5 even approach 1. The result illustrates the good performance of parameter search upon the MCMC evolution.

We now select the solutions with the highest objective values that are greater than 0.9 (i.e., Solutions 1–5), and compare their respective best model parameters as shown in Fig. 10. Apparently, model parameter values have noticeable discrepancies, which indicates the existence of multiple local optima in the objective surface. The new framework developed is indeed capable of capturing the underlying information of these local optima.

3.1.2.2. Target function approximation and further parameter identification. While the best model parameters identified directly from the abovementioned solutions indeed result in extremely high objective value, such as Solutions 4 (0.9937) and 5 (0.9991), they cannot be considered as final updating result. The reason is that a small number of data points, i.e., accepted samples and their objective values, cannot well characterize the true posterior PDF (Eq. (6)) especially when the parametric space is high-dimensional. To further enhance the accuracy of updating result, previous research [10] established a meta-model based on the scarce posterior PDF data points from MCMC, and then employed it to enrich the posterior PDF. The parameter estimation can then be conducted upon this enriched posterior PDF. It is worth pointing out that the underlying idea of MCMC actually allows an alternative for parameter optimization. Specifically, MCMC aims at constructing Markov chain that has desired distribution with respect to the target function/distribution [46]. The information of Markov chain in fact is fully represented by the accepted model parameter samples without

Table 1
MCMC parameters (Case 1).

w: number of samples for Monte Carlo	1000
r: number of best model parameter samples obtained through MC	50
t: pre-specified maximum number of iteration runs for each MCMC	2000
ε_C: distance threshold for determining initial parameter samples	0.23
ε_M: distance threshold for merge check of Markov chains	0.15
γ: default proposal distribution width	0.01
u: number of consecutive rejected steps for earlier termination	250
κ: burn-in length ratio	0.1

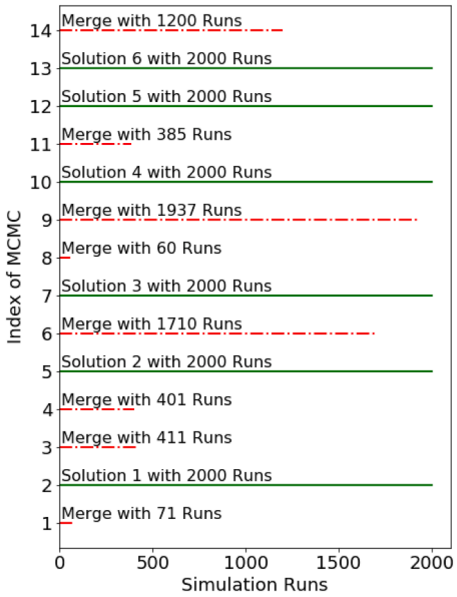

Fig. 8. MCMC evolution progresses.

the respective objective values. Therefore, the approximated distribution essentially is a histogram, representing the frequency of occurrence of the model parameter combinations.

A direct way to convert Markov chain into a histogram is briefly introduced as follows. For example, consider the i th solution/survived Markov chain with recorded information $\boldsymbol{\Theta}_{h\times g}^{(i)}$, where h is the length of the chain, and g is the number of model parameters to be updated, i.e., $g = 4$ in this current case. One can slice $\boldsymbol{\Theta}_{h\times g}^{(i)}$ into g column vectors, which then can be presented with histograms. In statistics, each histogram in the i th solution is used to represent the marginal PDF of certain model parameter, e.g., a marginal PDF denoted as $p(\boldsymbol{\alpha}_j)$, where $\boldsymbol{\alpha}_j$ is the j-th model parameter. In this case, we partition the entire range of $\boldsymbol{\alpha}_j$, i.e., [0, 1] into 20 uniform small bins, upon which the marginal PDFs of all model parameters are generated. While the statistical properties of such PDFs indeed indicate the probabilistic identification result, they cannot be directly utilized for identifying the best model parameters. The reason is that they are characterized based upon the assumption that all model parameters are independent. However, different model parameters essentially are coupled when characterizing the posterior PDF. The lack of coupling causes the inconsistency of frequency of occurrence at the same solution. To clarify this, we take Solution 1 as an example (Fig. 11). Obviously, the highest frequencies of occurrence of different model parameters are not identical.

Theoretically, the joint PDF is a quantity that can truly reflect the probability of model parameter combination to be the actual one. We thus use the joint PDF instead of the marginal PDF to conduct the subsequent probabilistic parameter identification. The mathematical relation between joint and marginal PDFs can be characterized as

$$p(\boldsymbol{\alpha}_j) = \int_{\vee\boldsymbol{\alpha}_1} .. \int_{\vee\boldsymbol{\alpha}_k(k\neq j)} .. \int_{\vee\boldsymbol{\alpha}_n} p(\boldsymbol{\alpha}_1, ..., \boldsymbol{\alpha}_j ... \boldsymbol{\alpha}_n) d\boldsymbol{\alpha}_1 .. d\boldsymbol{\alpha}_k .. d\boldsymbol{\alpha}_n \tag{10}$$

where $p(\boldsymbol{\alpha}_1, ..., \boldsymbol{\alpha}_j ... \boldsymbol{\alpha}_n)$ is the joint PDF. According to the above equation, the marginal PDF of the j-th model parameter is calculated as a multiple integral of joint PDF over the entire high-dimensional parametric space without the j-th dimension. For the sake of computation, we oftentimes approximate such integral using a discrete form, expressed as

$$p(\boldsymbol{\alpha}_j) = \sum_{\vee\boldsymbol{\alpha}_1} .. \sum_{\vee\boldsymbol{\alpha}_k(k\neq j)} .. \sum_{\vee\boldsymbol{\alpha}_n} p(\boldsymbol{\alpha}_1, ..., \boldsymbol{\alpha}_j ... \boldsymbol{\alpha}_n) \Delta\boldsymbol{\alpha}_1 .. \Delta\boldsymbol{\alpha}_k .. \Delta\boldsymbol{\alpha}_n \tag{11}$$

While the histogram is intuitive and convenient to characterize the joint PDF (Eq. (11)), it indeed has the weakness in representing the underlying data distribution because of its dependence with respect to the number of bins specified. Using too many bins can make analysis computationally costly especially for the multidimensional problem, while too few bins will overlook the important distribution feature, resulting in inaccurate data representation. Kernel density, as a non-parametric method, has demonstrated its capability to enable the efficient and smooth distribution estimation of multidimensional/multivariate data [52,53], and can address the issue of the histogram. The kernel function generally is symmetric, bounded and continuous, and its exact profile is determined by the so-called bandwidth that is to be optimized through the data training/fitting. Among various kernels, Gaussian kernel is most commonly used because it can produce very smooth data distribution [54]. In this case study, we employ the Gaussian kernel estimation to construct the joint posterior PDFs of the Markov chain information. According to the chain evolution (Fig. 9), Solution 6

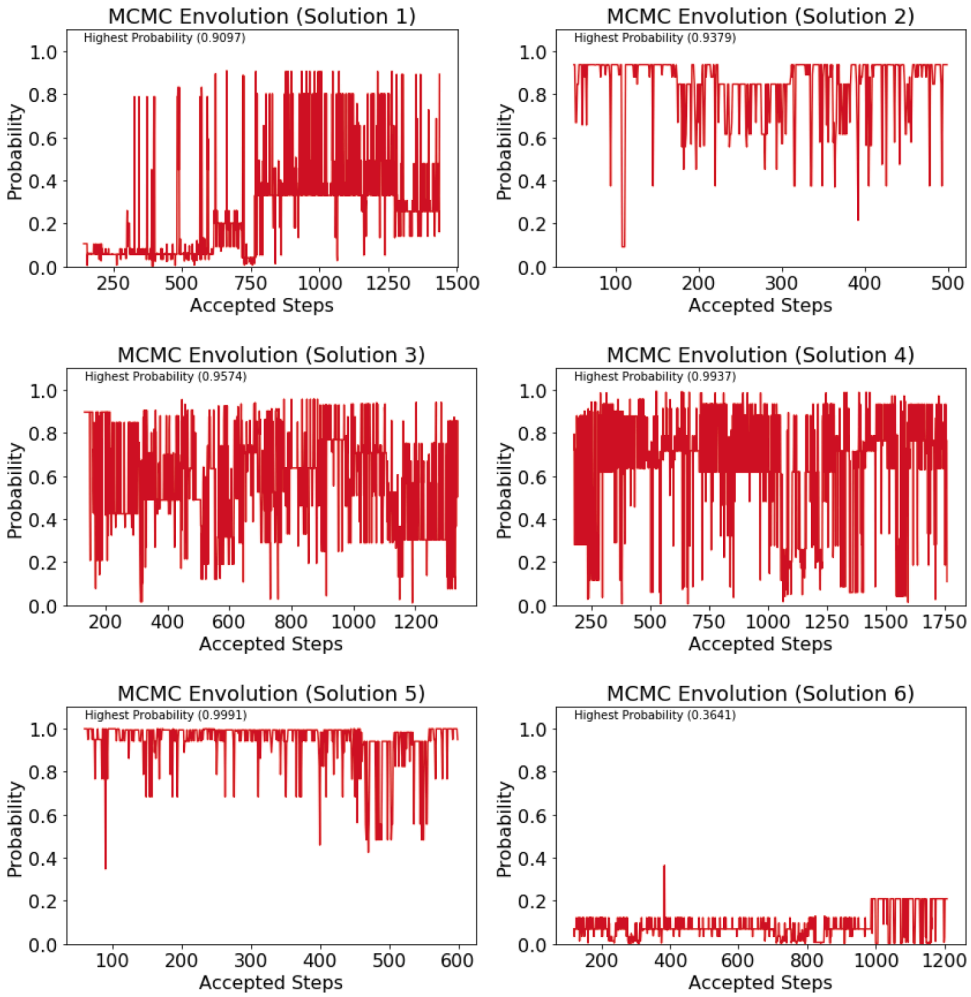

Fig. 9. MCMC evolution and optimization.

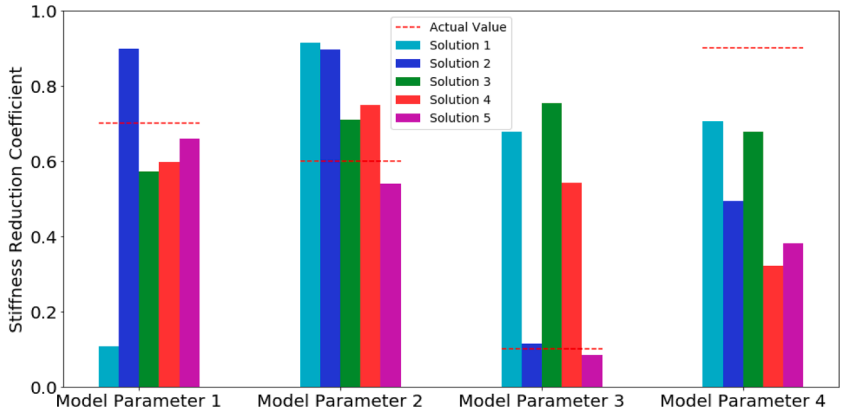

Fig. 10. Directly identified model parameters from the best 5 solutions through MCMC evolution.

certainly is not a potential local optimum due to the low probability yielded (i.e., 0.3641). As such, we only produce the joint PDFs of the other 5 Markov chains (probability higher than 0.9), as shown in Figs. 12–16. The multidimensional joint PDFs are converted to different univariate projections for the sake of visualization. This set of results not only provides a rational mean for parameter identification, but also probabilistically interprets the finding by taking into account the measurement and modeling uncertainties. For

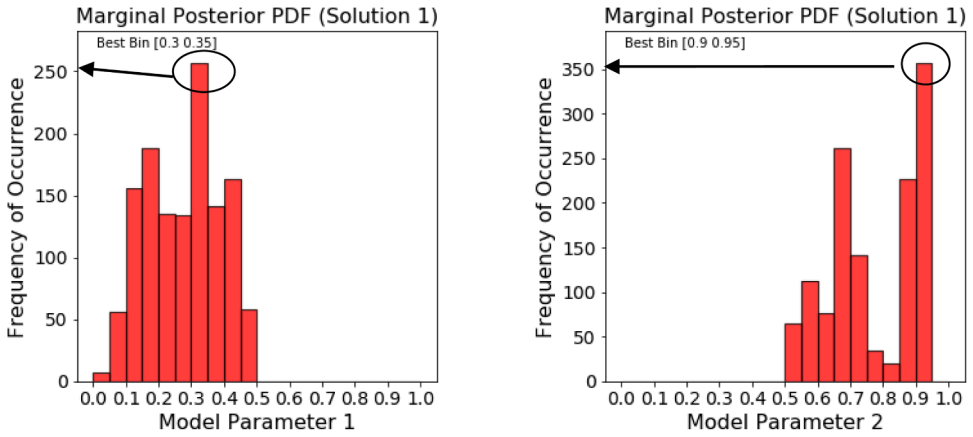

Fig. 11. Inconsistency of highest frequency of occurrence in marginal posterior PDF.

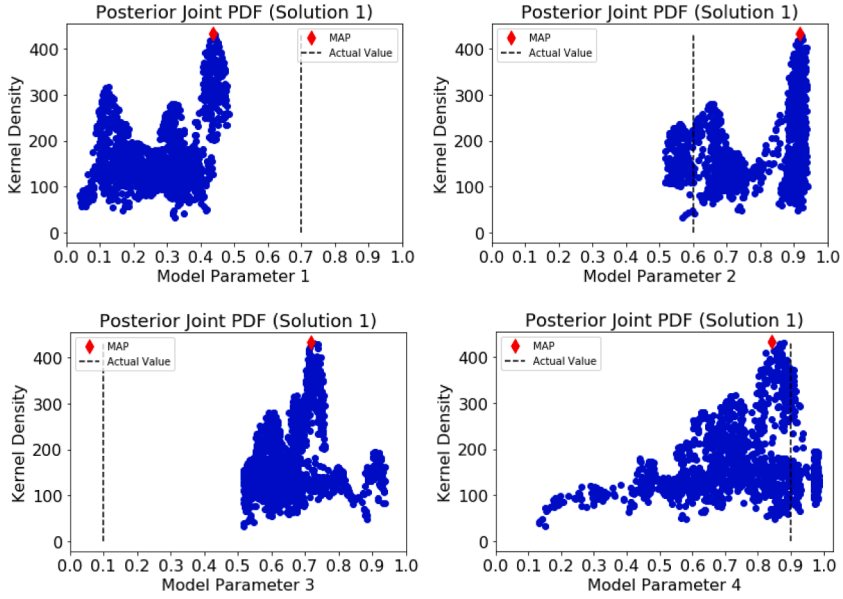

Fig. 12. Joint PDF constructed using kernel density estimation (Solution 1).

example, the confidence level of updating result is given.

We adopt the maximum a posteriori (MAP) estimation in Bayesian statistics [27,55,56] to identify the crisp model parameters of different solutions, shown in Figs. 12–16 and 17(a). The normalized Euclidean distance (NED) is formulated to evaluate the closeness between the identified and actual model parameters, given as

$$E_d = \frac{\| \boldsymbol{\alpha} - \overline{\alpha} \|}{\sqrt{n}} \tag{12}$$

where $\| \cdot \|$denotes the Euclidean norm, also known as the 2-norm. n is the number of model parameters or model parameter dimension, which is 4 in this case. $E_d$generally falls into [0,1]. The values in the legend of Fig. 17a indicates NED of identified model parameters of different solutions. The actual model parameters (i.e., 'ground truth') represented by the horizontal dash lines are used as baseline. Compared with other solutions, the parameters identified in Solution 5 are closer to the actual model parameters because of the smaller NED (indicated in the legend of Fig. 17a). Specifically, the identified model parameters 1, 2, 3 exactly match the respective actual model parameters. Only the identified model parameter 4 has certain discrepancy with respect to the actual value. From physical perspective, the model parameter 4 may be less sensitive to the selected modal responses. Overall, the result indicates the feasibility of the proposed framework.

To further illustrate the capacity of the framework for multiple local optima detection, we look into the modal responses of the identified model parameters in different solutions shown in Fig. 17(b). The ratio between the numerical and measured natural

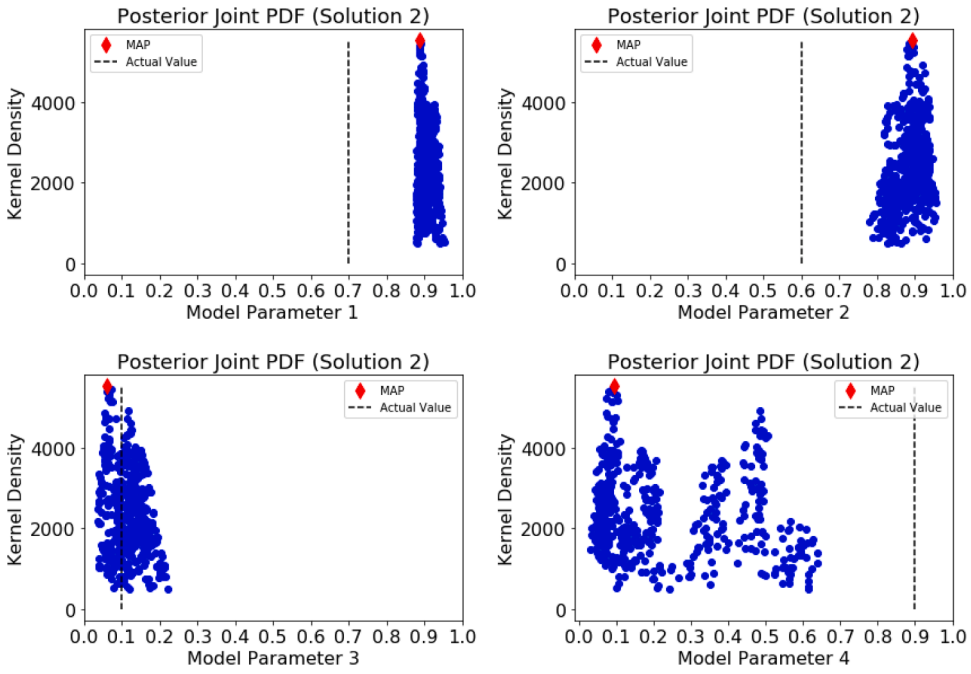

Fig. 13. Joint PDF constructed using kernel density estimation (Solution 2).

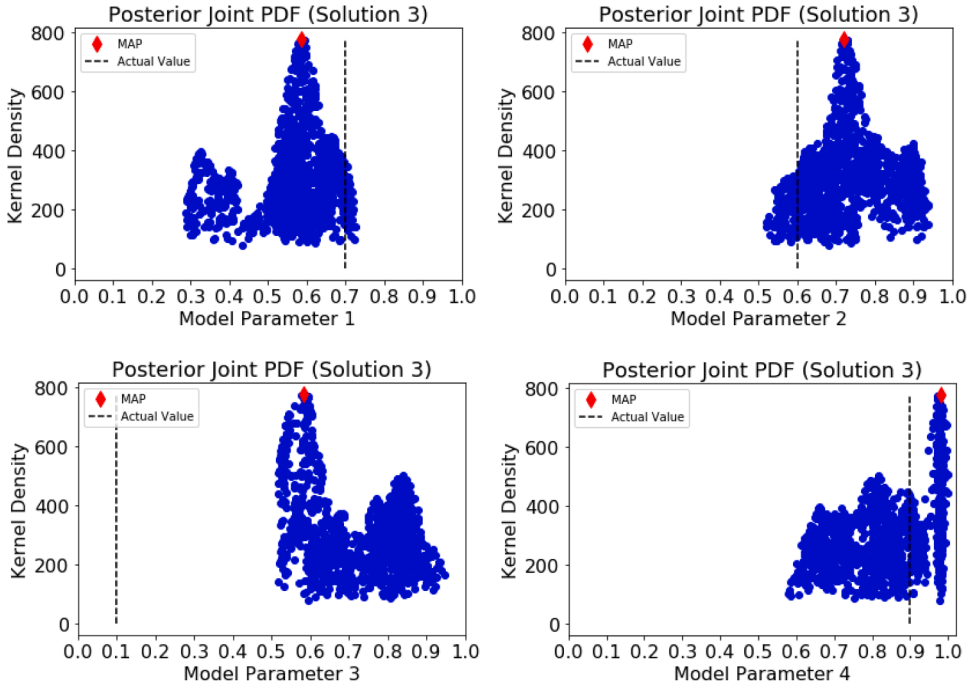

Fig. 14. Joint PDF constructed using kernel density estimation (Solution 3).

frequencies, and MAC are specifically utilized as the metrics for evaluating the response discrepancy. The closer the metric value to 1, the smaller the response discrepancy is. The result shows good match of almost all solutions except for Solution 2 where certain deviation exists. We then examine the spatial distances of the identified model parameters among different solutions (Fig. 17c), where the NED defined in Eq. (12) is also adopted. The contour plot (Fig. 17c) is symmetric, and the values on its diagonal line are all zero because of the same solution involved for comparison. As can be observed, the spatial distance between any two solutions generally is large, showing that the solutions are well-separated. Combining the observations of Fig. 17(b) and (c) again reflects that multiple local

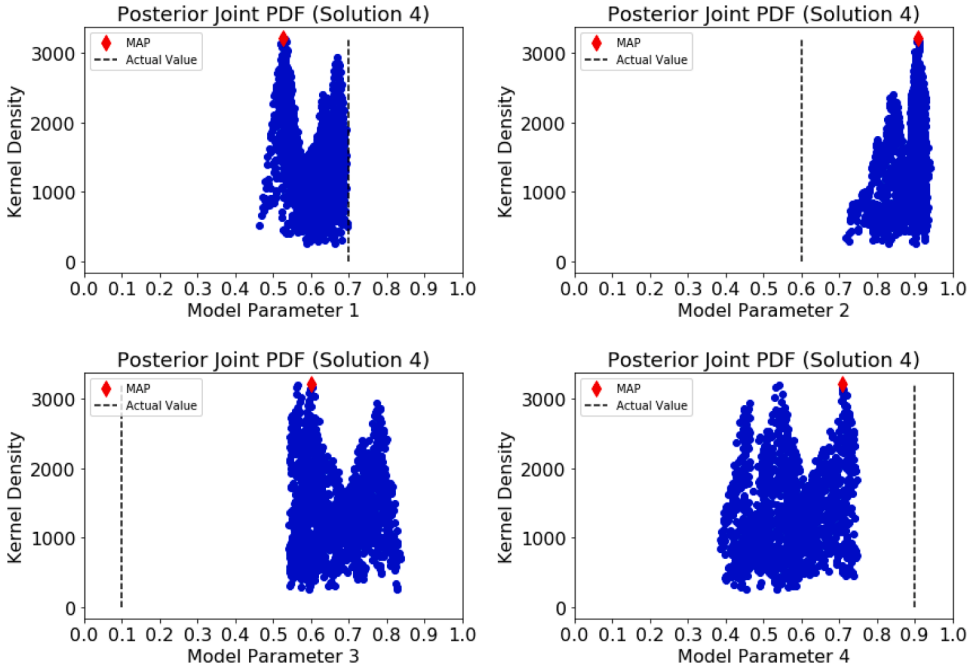

Fig. 15. Joint PDF constructed using kernel density estimation (Solution 4).

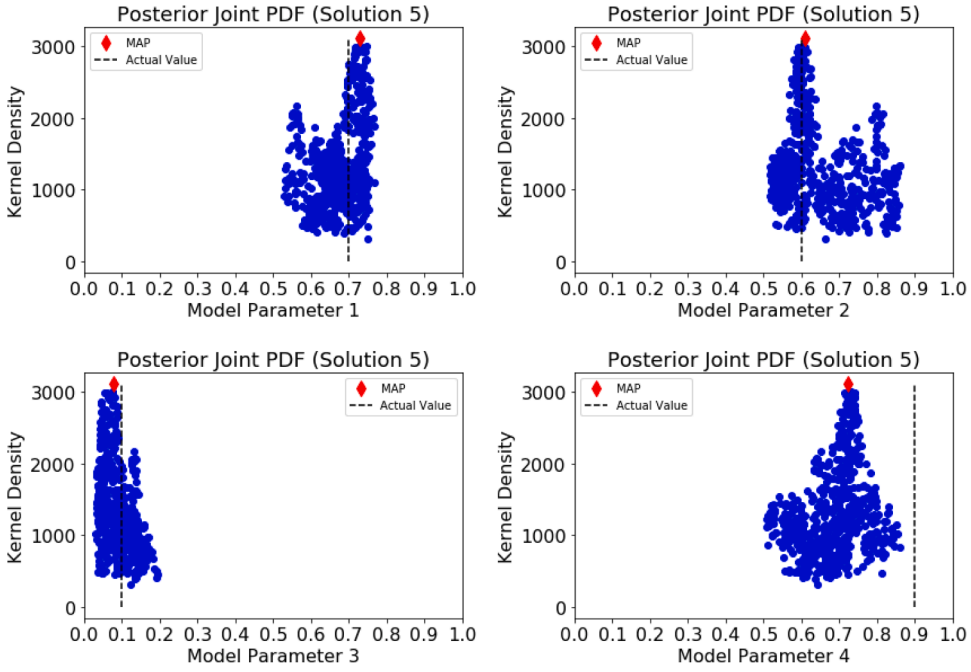

Fig. 16. Joint PDF constructed using kernel density estimation (Solution 5).

optima likely exist in this model updating problem, thereby providing the validation of the enhanced performance of this new framework.

3.1.2.3. Investigation of the effect of K-means clustering on model updating performance. As mentioned, the *K*-means clustering analysis plays a vital role in ensuring the good capability of the proposed approach for multiple local optima identification. To highlight this, here we carry out an additional case simulation without the clustering analysis and compare its result with the one shown above. To

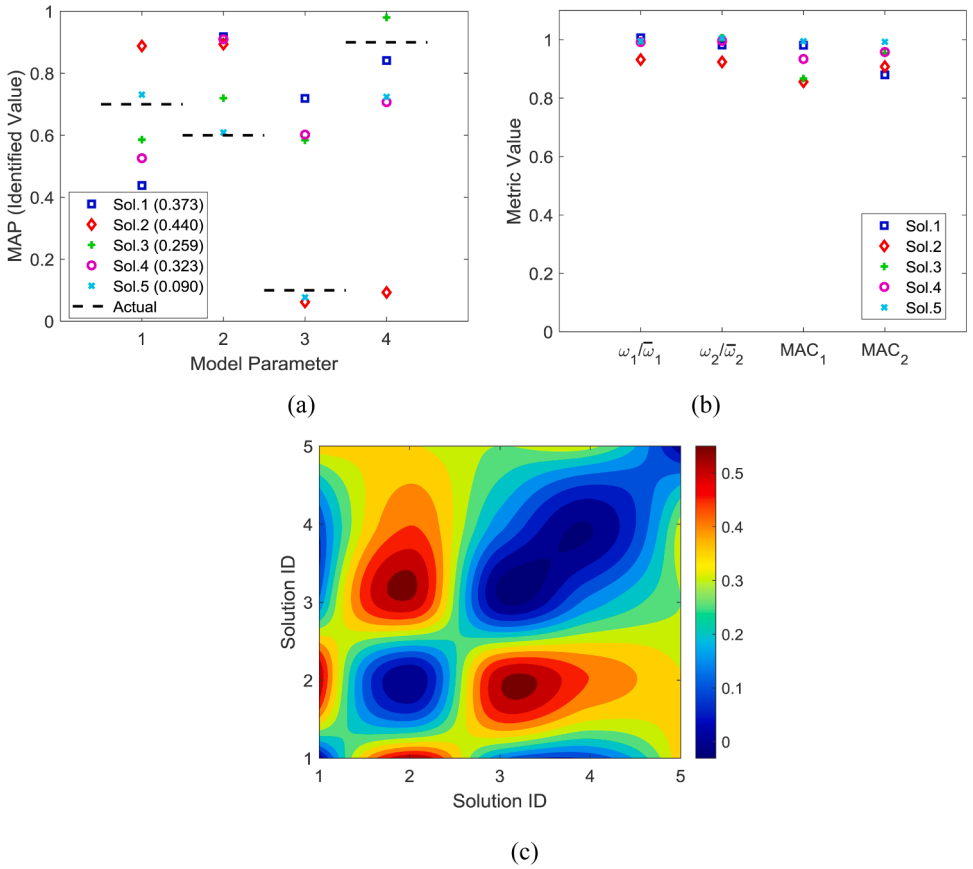

Fig. 17. Model updating results (a) identified model parameters of different solutions (The numerical value associated with the solution number indicates its normalized Euclidean distance with respect to actual parameters.); (b) absolute errors of natural frequencies and MACs of different solutions; (c) normalized Euclidean distances among the identified parameters of different solutions.

ensure the direct comparison, we choose the same number of initial positions of Markov chains, i.e., 14 for this new case, which are the top-ranking parameter samples sorted from the original Monte Carlo simulation result. With the same operating parameters defined in Table 1, the model updating is performed, which yields the result shown in Fig. 18. As compared with Fig. 17a, the number of solutions identified is reduced to 2. This implies that, without the clustering analysis the proposed approach fails to capture other possible local optima. The fundamental reason may be due to the closely distributed initial parameters for different Markov chains, some of which will easily converge to the same local optima. The clustering analysis that automatically generates the spatially well-separated initial

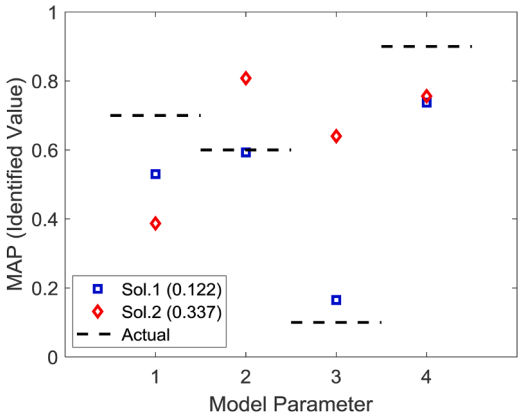

Fig. 18. Identified model parameters of different solutions without *K*-means clustering analysis (The numerical value associated with the solution number indicates its normalized Euclidean distance with respect to actual parameters.).

parameters over entire solution space can alleviate this issue. Additionally, the best solution, i.e., Solution 1, is found with the smallest NED yielded (indicated in the legend of Fig. 18). While the model parameters identified in Solution 1 tend to point to the respective actual parameters, the identifiability is worse than that using the clustering analysis.

Since the MH MCMC naturally incorporates the randomness into the model updating process, we execute 5 emulation runs with and without clustering analyses, respectively, for performance robustness assessment. The result is summarized in Table 2, which provides the consistent observation. Besides, the other local optimum, instead of the 'ground truth', much likely will be identified as the best solution if the clustering analysis is not employed. The results indicate the necessity of integrating the *K*-means clustering analysis for unleashing the power of the multiple Markov chains.

Overall, a series of results presented in this section clearly illustrate the capability of this framework to probabilistically identify multiple local optima. This in fact is advantageous in inverse analysis practice, in which the actual stiffness values at boundaries are unknown. The multiple solution options acquired can allow us to approach the 'ground truth' from various angles. One way of finalizing the solution option is to employ empirical knowledge and experience. For example, if we are only interested in response within certain frequency range, the best solution would be the one that yields the minimum difference between measurement and model prediction within that frequency range. In certain situations, we may gather additional information (e.g., additional modal information or additional sensors) to assist decision making.

3.2. Implementation scenario 2: stiffness reduction identification in plate structure

We then analyze the second implementation scenario, i.e., identification of stiffness reduction in a plate structure with large number of DOFs. As shown in Fig. 19(a), a plate structure with dimensions $0.4 \times 0.4 \times 0.005(\mathrm{m})$is investigated. It is clamped at two edges along the *x*-axis. The material constants are: Young's modulus 2.06×10^{11}Pa, mass density $7.85 \times 10^{3}\mathrm{kg}/\mathrm{m}^{3}$, and Poisson's ratio 0.3. The plate is meshed with 8-node solid element within ANSYS. The total number of DOFs is 10,086.

We divide the plate into 8 uniform segments along the *x*-axis, and our goal is to identify the change/reduction of stiffness in these segments, possibly caused by damage or material property non-uniformity. Therefore, this second implementation scenario applies to structural fault detection or model calibration with material property updating. We assign one stiffness reduction coefficient to each segment, so altogether we have 8 parameters to update, i.e., $n = 8$ in Eq. (2). In this simulated case, we assume the actual stiffness reduction coefficients, i.e., the 'ground truth', are known as $\overline{\alpha} = [0.2, 0.5, 0.6, 0.1, 0.6, 0.3, 0.2, 0.7]$. We assume only the information of the first two *z*-direction bending mode shapes is available. Moreover, we assume only 4 sensors are employed, so for the first two modes, only the amplitudes at 4 DOFs are measured. This leads to a model updating problem with severely limited and incomplete measurement. This scenario is considerably different from the first scenario as the number of DOFs in the baseline model is very large. Coupled with the incomplete measurement, the objective surface in Bayesian inference based model updating is very complicated. Fig. 19(b) illustrates the first *z*-direction bending mode shape of the structure, and shows 4 sensors that are uniformly distributed along the *x*-axis.

Similar to implementation scenario 1, in this second case a uniform distribution within the entire parametric space, i.e., [0, 1], is specified to characterize the prior PDF. Since in this second case we intend to utilize solely two incomplete bending mode shapes for model updating, we therefore only involve mode shape difference $\upsilon(\boldsymbol{\alpha})$ in the posterior PDF derivation following Eq. (6). It is worth noting that there indeed exist various ways of describing the difference between model prediction and measurement. In this second case, we adopt a new expression of mode shape difference, i.e., point-to point mode shape amplitude differences. The reason is that this can fully take advantage of the limited measurement information.

$$\upsilon(\boldsymbol{\alpha}) = \begin{bmatrix} \widehat{\psi}_{1,1} & \widehat{\psi}_{1,2} & \cdots & \widehat{\psi}_{1,q} \\ \widehat{\psi}_{2,1} & \widehat{\psi}_{2,2} & \cdots & \widehat{\psi}_{2,q} \\ \cdots & \cdots & \cdots & \cdots \\ \widehat{\psi}_{s,1} & \widehat{\psi}_{s,2} & \cdots & \widehat{\psi}_{s,q} \end{bmatrix} - \begin{bmatrix} \overline{\psi}_{1,1} & \overline{\psi}_{1,2} & \cdots & \overline{\psi}_{1,q} \\ \overline{\psi}_{2,1} & \overline{\psi}_{2,2} & \cdots & \overline{\psi}_{2,q} \\ \cdots & \cdots & \cdots & \cdots \\ \overline{\psi}_{s,1} & \overline{\psi}_{s,2} & \cdots & \overline{\psi}_{s,q} \end{bmatrix} = \begin{bmatrix} \Delta\psi_{1,1} & \Delta\psi_{1,2} & \cdots & \Delta\psi_{1,q} \\ \Delta\psi_{2,1} & \Delta\psi_{2,2} & \cdots & \Delta\psi_{2,q} \\ \cdots & \cdots & \cdots & \cdots \\ \Delta\psi_{s,1} & \Delta\psi_{s,2} & \cdots & \Delta\psi_{s,q} \end{bmatrix} \tag{13}$$

where *q* is the number of mode shapes and *s* is the number of measurement locations. To take into account the effect of measurement noise and modeling error, in this case the individual likelihood PDF for each mode shape amplitude is formulated as a normal distribution, given as

$$p(\Delta\psi_{j,k}|\boldsymbol{\alpha}) = \exp\left(\frac{-(\Delta\psi_{j,k})^2}{2\left(\eta_{j,k}\overline{\psi}_{j,k}\right)^2}\right) \tag{14}$$

Table 2
Identification results produced with and without clustering analyses.

		Run 1	Run 2	Run 3	Run 4	Run 5
With clustering	Potential solution number	5	4	4	5	5
	Best solution with smallest E_d	0.090	0.086	0.188	0.085	0.128
Without clustering	Potential solution number	2	3	3	3	3
	Best solution with smallest E_d	0.122	0.203	0.172	0.4182	0.113

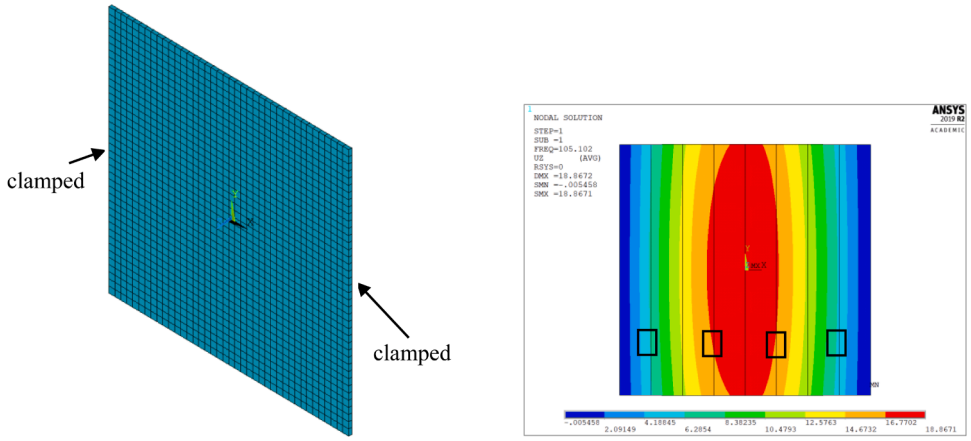

Fig. 19. Inverse analysis setup (a) FE model; (b) 1st z-direction bending mode shape contour plot of structure with 8-segment stiffness variations and 4 selected measurement locations (denoted by square).

where $\eta_{j,k}$ is the variance, indicating the uncertainty degree of the actual mode shape measurement $\overline{\psi}_{j,k}$. Here we set $\eta_{j,k}$ as 0.1 in this case. As discussed in Section 3.1.1, this value can adequately account for all the uncertainties and measurement noise. This likelihood PDF can ensure the higher probability of $\boldsymbol{\alpha}$ to be the actual model parameters when a smaller $\Delta\psi_{j,k}$is observed. Since all elements in $v(\boldsymbol{\alpha})$ have similar effect, we can write a final likelihood PDF in a multiplication form as

$$p(v(\boldsymbol{\alpha})|\boldsymbol{\alpha}) = \prod_{j=1}^{s}\prod_{k=1}^{q} p\left(\Delta\psi_{j,k}\middle|\boldsymbol{\alpha}\right) \tag{15}$$

Following the procedure outlined in Section 2, we can obtain the posterior PDF.

Once again, we specify the MCMC parameters and carry out the computation. Here it is worth nothing that we select a larger threshold value, i.e., $\varepsilon_C = 0.35$ than that of case 1 for clustering analysis because the dimension of parametric space in this case becomes higher. As a result, the spatial distance of different clusters generally will increase. In addition, a larger maximum number of iteration runs of MCMC, i.e., $t = 3{,}000$is adopted to enable the chain evolution convergence because of higher dimensional FE model and higher dimensional parametric space in this updating problem. Other parameters are kept the same as shown in Table 1.

By checking the Markov chain evolution history without the 'burn-in' period, all survived chains are supposed to point to the different local optima because the associated highest probability values are greater or around 0.9. By employing the kernel density estimation, we can obtain the joint posterior PDFs of different Markov chains, upon which the MAP is applied to identify the best model parameters. The result is tabulated in Table 3. The values in solution highlighted in bold font are very close to the actual values. Only the identified model parameter 5 has certain deviation with respect to the actual value. Moreover, while Solution 1 outperforms Solution 6 in terms of the highest objective value (i.e., probability) comparison, it appears to point to another local optimum where the measurement noise may play a role. Overall, the result indicates the consistent good updating performance of this new method. Once again, multiple solution options here allow us to carry out decision making possibly using additional information, e.g., non-destructive evaluation (NDE) in structural fault identification, to pinpoint the root cause.

4. Conclusions

This paper presents a new finite element (FE) inverse analysis framework using incomplete modal information in the presence of uncertainties. The framework is established upon the Bayesian inference through conducting parameter updating in terms of the posterior PDF. With limited measurement/target information, multiple local optima likely exist in the parametric space. To tackle the issue, we synthesize an enhanced Bayesian approach by incorporating multiple parallel, interactive and adaptive Markov chains. The

Table 3
Identified stiffness coefficients (MAP) from joint posterior PDFs using Gaussian kernel density estimation (Case 2).

	Para. 1	Para. 2	Para. 3	Para. 4	Para. 5	Para. 6	Para. 7	Para. 8	Highest probability
Solu. 1	0.268	0.724	0.635	0.392	0.497	0.267	0.481	0.249	0.9809
Solu. 2	0.332	0.476	0.135	0.685	0.482	0.221	0.540	0.144	0.9111
Solu. 3	0.021	0.323	0.215	0.443	0.867	0.047	0.582	0.672	0.9554
Solu. 4	0.126	0.125	0.556	0.373	0.0118	0.561	0.149	0.638	0.8733
Solu. 5	0.397	0.147	0.439	0.077	0.201	0.139	0.464	0.085	0.9024
Solu. 6	0.156	0.510	0.623	0.135	0.321	0.326	0.106	0.731	0.9688
Actual	0.2	0.5	0.6	0.1	0.6	0.3	0.2	0.7	

joint posterior PDFs constructed by the final survived Markov chains can be used to interpret the probabilistic updating results. We carry out the systematic case investigations through formulating different inverse analysis problems, i.e., boundary and material property updating of a dome and a plate structures, respectively. The results indicate that multiple optima can indeed be identified in terms of the joint posterior PDF computed via this numerical framework, and the 'ground truth' is included in the solution set with high probability. The statistical features of posterior PDF also indicate the confidence level of parameter estimation in the presence of uncertainties. This approach can be applied to a variety of inverse analysis problems such as fault identification, design optimization, and model updating.

CRediT authorship contribution statement

K. Zhou: Conceptualization, Methodology, Software, Validation, Formal analysis, Investigation, Data curation, Writing – original draft, Visualization. **J. Tang:** Conceptualization, Writing – review & editing, Supervision, Project administration, Funding acquisition.

Declaration of Competing Interest

The authors declare that they have no known competing financial interests or personal relationships that could have appeared to influence the work reported in this paper.

Acknowledgement

This research is supported in part by NSF under grant CMMI-1825324 and in part by a Space Technology Research Institutes grant (number 80NSSC19K1076) from NASA's Space Technology Research Grants Program.

Appendix. : pesudo code of ANSYS APDL

The APDL pseudo code for FE analysis under certain model parameter sample is given as follows.

```
Resume the baseline model (constructed beforehand)
RESUME,'dome_modal','db','D:\.....', 0,0
Read model parameter sample from intermediate file generated by external optimization code
*DIM,unSamp,1,n_inputs
*VREAD,UnSamp(1,1),input_data,txt,JIK,8,1
(8F8.4)
Modify model via changing stiffness values of springs at the boundaries in terms of new model parameter
    sample
/PREP7
*DO,JJ,1, n_inputs
R,JJ+1,(1-Unsamp(1,JJ))*10e24,0,0,0,
*ENDDO
Solve the analysis
NSEL, ALL
FINISH
/SOL
SOLVE
FINISH
Extract modal responses from defined measurement locations and write into intermediate file for optimization
    code
*DIM,NODEIDT,ARRAY,1,n_locations
*DIM MODE,ARRAY,n_modes,n_locations
*DIM MO,ARRAY,n_modes,1
*DIM,FREQ,ARRAY,1, n_modes
…
/POST1
*DO,I1,1, n_modes
*GET,FREQ(1,I1),MODE,SELORD(I1),FREQ
*ENDDO
*MWRITE,FREQ,output_Freq,TXT,JIK,n_modes,1
(2F9.5)
*DO,I,1,n_modes
SET,MO(I)
*DO,I1,1,n_locations
*GET, MODE(I,I1),NODE,NODEIDT(I1,1),U,Z
*ENDDO
*ENDDO
```

(*continued on next page*)

(*continued*)

*MWRITE,MODE,output_Mode,TXT,JIK,n_locations,n_modes (4F13.5)

Note: The geometry, mesh and fixed boundaries etc., have been set up in the baseline model. Therefore, in the model updating APDL script, there is no need to re-define those properties/variables.

References

[1] C. Traylor, M. DiPaola, D.J. Willis, M. Inalpolat, A computational investigation of airfoil aeroacoustics for structural health monitoring of wind turbine blades, Wind Energy 23 (2020) 795–809.
[2] M. Fronk, K. Eschen, K. Starkey, R.J. Kuether, A. Brink, T. Walsh, W. Aquino, M. Brake, Inverse methods for characterization of contact areas in mechanical systems, Nonlinear Dyn. 1 (2017) 45–56. Conference Proceedings of the Society for Experimental Mechanics Series. Springer, Cham.
[3] W.J. Yan, D. Chronopoulos, C. Papadimitriou, S. Cantero-Chinchilla, G.S. Zhu, Bayesian inference for damage identification based on analytical probabilistic model of scattering coefficient estimators and ultrafast wave scattering simulation scheme, J. Sound Vib. 468 (2020), 115083.
[4] D. Giagopoulos, A. Arailopoulos, V. Dertimanis, C. Papadimitriou, E. Chatzi, K. Grompanopoulos, Structural health monitoring and fatigue damage estimation using vibration measurements and finite element model updating, Struct. Health Monit. 18 (2019) 1189–1206.
[5] H. Tran-Ngoc, L. He, E. Reynders, S. Khatir, T. Le-Xuan, G. De Roeck, T. Bui-Tien, M. Abdel Wahab, An efficient approach to model updating for a multispan railway bridge using orthogonal diagonalization combined with improved particle swarm optimization, J. Sound Vib. 476 (2020), 115315.
[6] E.M. Hernandez, D. Bernal, Iterative finite element model updating in the time domain, Mech. Syst. Signal Process. 34 (2013) 39–46.
[7] X. Chang, S. Chai, R.J. Allemang, L.J. Li, A new iterative model updating method using incomplete frequency response function data, J. Sound Vib. 333 (2014) 2443–2453.
[8] T. Wang, H. He, W. Yan, G.P. Chen, A model-updating approach based on the component synthesis method and perturbation analysis, J. Sound Vib. 433 (2018) 349–365.
[9] W. Wang, J.E. Mottershead, C. Mares, Mode-shape recognition and finite element model updating using the Zernike moment descriptor, Mech. Syst. Signal Process. 23 (2009) 2088–2112.
[10] Y. Wang, M. Liang, J. Xiang, Damage detection method for wind turbine blades based on dynamics analysis and mode shape difference curvature information, Mech. Syst. Signal Process. 48 (2014) 351–367.
[11] K. Zhou, J. Tang, Highly efficient probabilistic finite element model updating using intelligent inference with incomplete modal information, Trans. ASME J. Vib. Acoust. 138 (2016), 051016.
[12] N. Moaveni, J.P. Conte, F.M. Hemez, Uncertainty and sensitivity analysis of damage identification results obtained using finite element model updating, Comput.-Aided Civ. Infrastruct. Eng. 24 (2009) 320–334.
[13] H.H. Khodaparast, J.E. Mottershead, K.J. Badcock, Interval model updating with irreducible uncertainty using the Kriging predictor, Mech. Syst. Signal Process. 25 (2011) 1204–1226.
[14] J.L. Beck, L.S. Katafygiotis, Updating models and their uncertainties. I: Bayesian statistical framework, J. Eng. Mech. 124 (1998) 455–461.
[15] J.E. Mottershead, M. Link, M.I. Friswell, The sensitivity method in finite element model updating: a tutorial, Mech. Syst. Signal Process. 25 (2011) 2275–2296.
[16] Y. Liu, K. Zhou, Y. Lei, Using Bayesian inference towards identifying gas species and concentration from high temperature resistive sensor array data, J. Sens. 2015 (2015), 351940.
[17] G. Yan, H. Sun, A non-negative Bayesian learning method for impact force reconstruction, J. Sound Vib. 457 (2019) 354–367.
[18] Z. Chen, R. Zhang, J. Zheng, H. Sun, Sparse Bayesian learning for structural damage identification, Mech. Syst. Signal Process. 140 (2020), 106689.
[19] J. Lee, J. Son, S. Zhou, Y. Chen, Variation source identification in manufacturing processes using Bayesian approach with sparse variance components prior, IEEE Trans. Automat. Sci. Eng. 17 (2020) 1469–1485.
[20] H.P. Wan, Y.Q. Ni, A new approach for interval dynamic analysis of train-bridge system based on Bayesian optimization, J. Eng. Mech. 146 (2020), 04020029.
[21] Y. Xin, H. Hao, J. Li, Z.C. Wang, H.P. Wan, W.X. Ren, Bayesian based nonlinear model updating using instantaneous characteristics of structural dynamic responses, Eng. Struct. 183 (2019) 459–474.
[22] Z. Xia, J. Tang, Characterization of dynamic responses of structures with uncertainty by using Gaussian process, Trans. ASME J. Vib. Acoust. 135 (2013), 051006.
[23] S.S. Jin, H.J. Jung, Sequential surrogate modeling for efficient finite element model updating, Comput. Struct. 168 (2016) 30–45.
[24] J.L. Beck, S.K. Au, Bayesian updating of structural models and reliability using Markov Carlo simulation, J. Eng. Mech. 128 (2002) 380–391.
[25] J. Ching, Y.C. Chen, Transitional Markov chain Monte Carlo method for Bayesian model updating, model class selection, and model averaging, J. Eng. Mech. 133 (2007) 816–832.
[26] H.F. Lam, J. Yang, S.K. Au, Bayesian model updating of a coupled-slab system using field test data utilizing an enhanced Markov chain Monte Carlo simulation algorithm, Eng. Struct. 102 (2015) 144–155.
[27] H.F. Lam, S.A. Alabi, J.H. Yang, Identification of rail-sleeper-ballast system through time-domain Markov chain Monte Carlo-based Bayesian approach, Eng. Struct. 140 (2017) 421–436.
[28] I. Behmanesh, B. Moaveni, Probabilistic identification of simulated damage on the Dowling Hall footbridge through Bayesian finite element model updating, Struct. Control Health Monit. 22 (2015) 463–483.
[29] Z. Niu, Frequency response-based structural damage detection using Gibbs sampler, J. Sound Vib. 470 (2020), 115160.
[30] Y. Choe, E. Byon, N. Chen, Importance sampling for reliability evaluation with stochastic simulation models, Technometrics 57 (2015) 351–361.
[31] S. Brooks, A. Gelman, G. Jones, X.L. Meng, Handbook of Markov Chain Monte Carlo, Chapman and Hall/CRC, 2011.
[32] S. Biswal, A. Ramaswamy, Finite element model updating of concrete structures based on imprecise probability, Mech. Syst. Signal Process. 94 (2017) 165–179.
[33] H. Sun, A. Mordret, P.A. Prieto, M.N. Toksoz, O. Buyukozturk, Bayesian characterization of buildings using seismic interferometry on ambient vibrations, Mech. Syst. Signal Process. 85 (2017) 468–486.
[34] F. Liang, C. Liu, R. Carroll, Advanced Markov Chain Monte Carlo Methods: Learning from Past Samples, Wiley, 2010.
[35] C. Ji, S.C. Schmidler, Adaptive Markov chain Monte Carlo for Bayesian variable selection, J. Comput. Graph. Stat. 22 (2013) 708–728.
[36] H.F. Lam, J. Hu, F.L. Zhang, Y.C. Ni, Markov chain Monte Carlo-based Bayesian model updating of a sailboat-shaped building using a parallel technique, Eng. Struct. 193 (2019) 12–27.
[37] Y. Xia, H. Hao, Statistical damage identification of structures with frequency changes, J. Sound Vib. 263 (2003) 853–870.
[38] X.L. Liu, Behavior of derivatives of eigenvalues and eigenvectors in curve veering and mode localization and their relation to close eigenvalues, J. Sound Vib. 256 (2002) 551–564.
[39] M. Brehm, V. Zabel, C. Bucher, An automatic mode pairing strategy using an enhanced modal assurance criterion based on modal strain energies, J. Sound Vib. 329 (2010) 5375–5392.
[40] H. Sun, O. Buyukozturk, Probabilistic updating of building models using incomplete modal data, Mech. Syst. Signal Process. 75 (2016) 27–40.
[41] P. Dostert, Y. Efendiev, T.Y. Hou, Multiscale finite element methods for stochastic porous media flow equations and application to uncertainty quantification, Comput. Methods Appl. Mech. Eng. 197 (2008) 3445–3455.

[42] Y. Huang, J.L. Beck, H. Li, Bayesian system identification based on hierarchical sparse Bayesian learning and Gibbs sampling with application to structural damage assessment, Comput. Methods Appl. Mech. Eng. 318 (2017) 382–411.
[43] F. Pedregosa, G. Varoquaux, A. Gramfort, V. Michel, B. Thirion, O. Grisel, M. Blondel, P. Prettenhofer, R. Weiss, V. Dubourg, J. Vanderplas, A. Passos, D. Cournapeau, M. Brucher, M. Perrot, E. Duchesnay, Scikit-learn: machine Learning in Python, J. Mach. Learn. Res. 12 (2011) 2825–2830.
[44] L. Liberti, C. Lavor, Euclidean Distance Geometry: an Introduction, Springer, 2017.
[45] Y. Liu, Z. Li, H. Xiong, X. Gao, J. Wu, Understanding of internal clustering validation measures, IEEE Int. Conf. Data Mining 5694060 (2010) 911–916.
[46] J.S. Teixeira, L.T. Stutz, D.C. Knupp, A.J. Silva Neto, A new adaptive approach of the Metropolis-Hastings algorithm applied to structural damage identification using time domain data, Appl. Math. Model. 82 (2020) 587–606.
[47] D.P. Kroese, T. Taimre, Z.I. Botev, Handbook of Monte Carlo Methods, Wiley, 2011.
[48] K. Zhou, J. Tang, Uncertainty quantification in structural dynamic analysis using two-level Gaussian processes and Bayesian inference, J. Sound Vib. 412 (2018) 95–115.
[49] I. Behmanesh, B. Moaveni, G. Lombaert, C. Papadimitriou, Hierarchical Bayesian model updating for structural identification, Mech. Syst. Signal Process. 64-65 (2015) 360–376.
[50] A. Teughels, G. De Roeck, Structural damage identification of the highway bridge Z24 by FE model updating, J. Sound Vib. 278 (2004) 589–610.
[51] A. Nozari, I. Behmanesh, S. Yousefianmoghadam, B. Moaveni, A. Stavridis, Effects of variability in ambient vibration data on model updating and damage identification of a 10-story building, Eng. Struct. 151 (2016) 540–553.
[52] ANSYS Inc., Ansys® Academic Research Mechanical, Release 19.2, Canonsburg, PA, USA, 2018.
[53] T.A. O'Brien, K. Kashinath, N.R. Cavanaugh, W.D. Collins, J.P. O'Brien, A fast and objective multidimensional kernel density estimation method: fastKDE, Comput. Stat. Data Anal. 101 (2016) 148–160.
[54] D.W. Scott, Multivariate Density Estimation: Theory, Practice, and Visualization, Wiley, 1992.
[55] M. Kristan, A. Leonardis, D. Skocaj, Multivariate online kernel density estimation with Gaussian kernels, Pattern Recognit. 44 (2011) 2630–2642.
[56] A. Das, N. Debnath, A Bayesian model updating with incomplete complex modal data, Mech. Syst. Signal Process. 136 (2020), 106524.